Master Thesis in Geosciences

THE INFLUENCE OF SULPHUR EMISSIONS FROM SHIP TRAFFIC ON CLOUDS AND CLIMATE

KAI KOMBO HAMAD

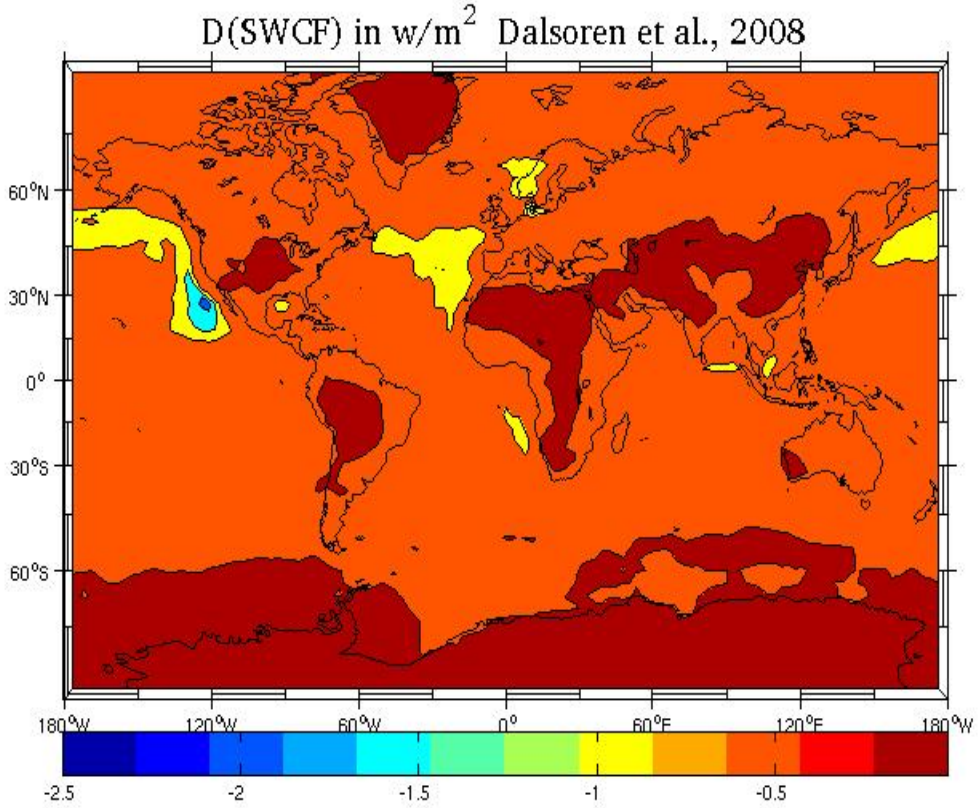

UNIVERSITY OF OSLO

FACULTY OF MATHEMATICS AND NATURAL SCIENCES

Blank page, for double side paper print.
Remove for digital publishing

THE INFLUENCE OF SULPHUR EMISSIONS FROM SHIP TRAFFIC ON CLOUDS AND CLIMATE

Kai Kombo Hamad

Master Thesis in Geosciences

Discipline: Meteorology and Oceanography

Department of Geosciences

Faculty of Mathematics and Natural Sciences

UNIVERSITY OF OSLO

[28 May 2010]

ABSTRACT

The growth of the international ship trade has raised the great concern about the impact of the ship emitted pollutants to the clouds and climate, air quality est. Apart from emitting large extents of sulphur dioxide which is oxidized to sulphate particles in the atmosphere; also ships emit full spectrum range of organics and non organics. These sulphate particles either by their own or in mixture with other emitted organics interrupt the earth's radiation budget either directly or indirectly (via cloud properties) resulting in a net cooling effect on the atmosphere.

The study used the Community Atmospheric Model version three or CAM3.0 with detailed aerosol and cloud microphysical scheme to investigate the effects of international shipping traffic on clouds and climate. The model simulation results show that the top of atmosphere ship induced indirect effect is highly uncertain and model based. The model calculated global mean value of $-0.063 Wm^{-2}$ to $-0.121 Wm^{-2}$, which contribute to about 3.3% to 6.4% of the total indirect effect of anthropogenic aerosols is three times lower than that of E5/M1-MADE. Particle organic matter (POM) and black carbon from fossil fuels (BC) contribute to about 8% and 16% of the short wave radiative flux due to shipping. Seasonally, the highest short wave radiative flux response due to shipping is on JJA which contribute to about $-0.187 Wm^{-2}$ to $-0.102 Wm^{-2}$ or 39% to 40% depending on the inventory. Over the Southern Hemisphere ship induced short wave radiative flux show an increasing trend of about $-0.021 Wm^{-2}$ to $-0.065 Wm^{-2}$ or 17% to 27% of the global mean ship induced short wave cloud forcing.
On microphysical properties the simulation results show an increase of only 3% to 5% for cloud droplet number concentrations over the low marine liquid water clouds of Atlantic and Pacific Oceans, where as the percentage changes in liquid water path has shown to be less than 1% both globally and regional. Model results yield a ship induced sulphate burden of 3.0% to 3.8%, and ship contributed BC and POM of 2.0% and 0.5%. For the lower most boundary layer of Atlantic Ocean, the model results reveals an increase of only 9% in particle number concentration of the Aitken mode (less than 0.1μm)), which is accompanied with the decrease in the weighted geometrical mean diameter of about 0.050μm to 0.055μm depending on the inventory**,** and only 3% increase in the accumulation mode particle number concentration which are approximately five times lower than that of E5/M1-MADE. The study results show a contribution of 9% to 17% of the total indirect radiative forcing (RF) of ($-0.7 Wm^{-2}$) of the year 2005 (IPCC, 2007) and 4% to 7% of the total anthropogenic sulphate AIE (i.e. $-1.8 Wm^{-2}$ for first kind and second kind) calculated by (Kristjansson et al., 2002). For the shipping the study contributes to 15% to 30% of the total indirect RF of ($-0.409 Wm^{-2}$) of the year 2005 (Eyring et al., 2009). Though the model simulations of AIE due to shipping has been affected by uncertainties based on models and shipping emission inventories, but this results show a significant contribution to the cooling effect of the climate. Based on this contribution the study generally conclude that the growing problem of ship induced effects on clouds and climate, which is enhanced by the growth of world sea-trade needs special scientific attention and considerations.

Acknowledgement

The completion of this work has been influenced by number of people who volunteered their assistance either ideally or technically, and even motivation. I would like to thank the Norwegian State Educational Loan Fund under their Quota Programme for providing full sponsorship of my master programmed, and all whom they participate in one way or another to the completion of this study.

First and the most is my supervisor Jon Egill Kristjansson, not only for motivating me towards this interesting and exciting topic, as well as for his spirit of providing skillful and relevant guidance towards this study, but also for giving me hope whenever I feel engulfed with social related problems.

Secondly I would like to thank all my core supervisors for their support whenever I get stack, but special thanks should go to Corrina Hoose whom she not only orients me to know and use the CAM3.0 model but also for her spirit to check the consistency and correctness of my results from step to step, as well as for her challenging questions which makes me to have an extensive reading and acquiring great understanding of my study.

A big thank should go to Øyvind Seland for helping me with all kinds of model related aspects (including finding of correct data, removing or adding of data into the model etc) as well as his advice whenever I contact him. I would also like to thank F. Dentener and Stig B. Dalsoren for their good work of modeling ship emission inventories which are now in use for advanced studies. Furthermore I would like to thank all MetOs computing stuff, and my fellow students for assisting me with help on computer- related problems.

Endless thanks should be forwarded to my lovely wife (Asha Moh'd Mmanga) and children (including Ismail, Zulk, and Hamad est**.**) for motivating me to complete my studies and for their calmness with tired less waiting for the whole time of my absence.

LIST OF CONTENTS

LIST OF TABLES

LIST OF FIGURES

CHAPTER ONE

1. Introduction

The emissions of anthropogenic sulphur dioxide which is oxidized to sulphate aerosols from main sources including industry, aircraft and shipping has increased the induced forcing due to human interaction with the environment, by increasing the aerosol column number concentration (Lauer et al., 2007; Eyring et al., 2009: Sekiguchi et al., 2003). This have induced the interruption of the earths radiative balance (due to scattering of the light by sulphate aerosols) by altering the microphysical and radiative properties of clouds (sulphate acts as an efficient cloud condensation nuclei (CCN) in clouds) Lauer et al., 2007; Kristjansson et al., 2002; Hasselmann et al., 1995; Mitchell et al., 1995a; Johns et al., 1997; Meehl et al., 1996, est.

Not only the re-distribution of radiative balance, but also anthropogenic sulphate aerosol has been confirmed to have significant potential of modifying greenhouse warming (Taylor and Penner 1994; Mitchell et al., 1995b; Roeckner et al., 1995; Erickson et al., 1995; Treut et al., 1996 where as the net combined effect is to cool the climate (Storelvmo et al., 2006) .

Anthropogenic sulphate aerosols from shipping might cause both direct and indirect effects (Lauer et al., 2007), but for the scope of this study we will only confine ourselves on the indirect effects of sulphate aerosols on clouds (first kind and second kind) Twomey (1997); Albrecht (1989). The injected CCN in a cloud cause the change in droplet size due to increased number of CDNC Lauer et al., 2007, which induces the change in LWP i.e. (reshaping the microphysical and radiative properties of cloud) causing global net cooling effect. Furthermore the decrease in droplet size due to competition of aerosols on moisture limits the precipitation efficiency or the cloud lifetime Albrecht (1989), thereby alters or enhances the increase in cloud albedo or reflectivity Kristjansson et al., 2005; 2002; Rosenfeld et al., 2002; Lauer et al., 2007:

The main goal of this work is to investigate the influence of emissions from ship traffic on clouds and cloud radiative forcing, thereby estimating (quantify) their contribution to the aerosol indirect effect (AIE). Globally the magnitude of the shipping effect can be seen by considering all emission data from ships at sea, in ports and deep sea observations, which has been reported to contribute to about 9584Kt/year of SO_2 which is oxidized to sulphate particles Dalsoren et al., 2008. On average sulphur content in marine heavy fuels used by most ocean going ships ranges from (2.4–2.7%) EPA, 2006; Endresen et al., 2005, causing the SO_2 emission to be high as exampled by Eyring et al., 2009 that the 2001 SO_2 emission ranges between 8.7 and 12.03Tg(SO_2)

Other studies have given different results for the contribution of shipping to sulphur emission, where by Lauer et al., 2007 indicate that shipping contribute around 8% of the present total anthropogenic SO_2 emissions. For the surface levels concentrations, Olivier et al., 2005 and Dalsoren et al., 2008 come up with a contribution of 20–70% for SO_2 and 40–90% for NO_2 for major shipping lanes, where as Capaldo et al., 1999 come up with the finding that the anthropogenic sulphur emission from ships are comparable to biogenic dimethyl sulphide (DMS), and the annual sulphur emissions from ships equals (or exceed) those of adjacent land based sources.

The effectiveness of an aerosol as a CCN depends on its size and its response to water, but as far as the shipping emission inventories for different compounds including organic, non organic, Volatile Organic Compounds, BC (Black Carbon) are concerned, SO_2 emissions from shipping are oxidized to sulphate in aqueous phase (in cloud droplets and sea salt particles) and also in the gas phase by the OH radical Dalsoren et al., 2008.

Most studies has accepted that, most models treat organic carbon as partial hygroscopic i.e. they can act as CCN when externally mixed at high supper saturation (Storelvmo et al., 2006; Kristjansson et al., 2002; Lohmann et al., 2004), whereby in the same concern of estimating the supper saturation level for organics Dick (2000) and Gysel et al., 2004 have shown that their water uptake (CCN activity) can be even at relative humidity less than 100%.
On the process of increasing the ability of the droplet to take up water (aerosol activation scheme) organics (POM and BC) may decrease the surface tension of a droplet (Anttilla and Kerminen, 2002 and Facchini et al., 1996), though other studies have shown that surface tension could potentially counteract the delayed activation improved by reduced particle solubility (Shulman et al., 1996).

This explains why we have to put more attention on studying radiative and microphysical effects of ongoing shipping emission to clouds because it has been recognized as a growing problem by both policymakers and scientists (Eyring et al., 2009), where the recent annual growth rates in total seaborne trade in ton-miles have been 5.2% on average from 2002 to 2007 (Fearnleys, 2007), causing a significant annual increase in the fuel consumption up to 217Mt by 2004 (Dalsoren et al., 2008). Also due to the fact that there is significant uncertainty on quantifying the effect of sulphate aerosols on clouds microphysics caused by high uncertainty in emission inventories (collection and consideration methods of fuel consumption data), fueled by little attention given to the growing world sea trade (Eyring et al., 2005b; Lauer et al., 2007) we have been convinced to contribute our efforts on this area of study.

Among other reasons as to why this research problem is of interest is the fact that the indirect aerosol effect by ship emissions is not highly researched, only rough estimates for sulphate

plus organic material particles (OC) from global model simulations without detailed aerosol and cloud physics (Capaldo et al., 1999) are currently available. The overall indirect effect due to international shipping taking into account aerosol nitrate, black carbon, particulate organic matter and aerosol liquid water in addition to sulphate as well as detailed aerosol physics and aerosol cloud interaction has not been assessed in a fully consistent manner yet (Lauer et al., 2007).

On the ongoing efforts of having well documentation of the microphysical and radiative effects of sulphur emissions from ships, Lauer et al., 2007 using the E5/M1-MADE General Circulation Model (GCM) estimated both the direct and indirect effects of shipping emission (including the sulphate, nitrate, POM, BC est.) over the coastal as well as deep sea for Atlantic and Pacific Ocean. Apart from the global mean changes of these effects, but his key interest was to examine and estimate both microphysical and radiative effects of these pollutants on cloud for the lower boundary marine liquid water clouds on lower troposphere level of approximately 1.5km altitude. As the way to reach his goal and addressing or limiting the emission uncertainty he used three different emission inventories including Wang et al., 2007; Dentener et al., 2006 and Eyring et al., 2005a.

On the same grounds of studying, estimating and quantifying the effects of ongoing ship traffic on environments and health, Dalsoren et al., 2008 used the global Chemical Transport Model (CTM) to strengthen the accuracy and validity of activity based ship emissions modeling, using the improved modeling tools and data sets. In his study he come up with the up-to-date ship emission inventory (which is now known as Dalsoren et al., 2007 ship emission inventory) and the quantified environmental impacts of the constituents of the ship emission including SO_2, NO_2, BC, OC and compounds associated from NO_x est.

In this study two inventoris, Dentener et al., 2006 and Dalsoren et al., 2008 with back ground model cloud (no ship emission) were used to investigate (estimating and quantifying) the influence of sulphate emissions on clouds and climate. The study is based both on global effects and localized regions of interest (the grids of the areas are defined in section (4.4.1)) over the high ship traffic areas in the Pacific and Atlantic Ocean. On achieving the stated goal the Community Atmospheric Model version 3 (CAM3.0) with detailed aerosol and cloud microphysics is used as a tool to study the indirect sulphate aerosol effect caused by the international shipping. For the performance evaluation of our model (C AM3.0) results we have compared our findings to that E5/M1-MADE and state the reasons on areas where the results from the two models differs.

In order to reach the above stated objective the model output parameters including cloud droplet number concentration (CDNC and CDNCINT), cloud integrated liquid water content (LWP), cloud droplet effective radius (R_e), aerosol optical depth (AOD) at 550nm, cloud

optical depth (COD), cloud albedo (CA), sulphate burden and sulphate nucleation rate, amount of radiation, sulphur emissions, short wave cloud forcing (SWCF) and long wave cloud forcing (LWCF) were investigate. The reasons for choosing these model output parameters is the fact that overall aerosol impact of top of atmosphere (TOA) indirect effect (first and second kinds) is mainly determined by the relative and percentage change in LWP and droplet effective radius, which in turn depends on amount of CCN inject in the cloud, super saturation level as well as cloud liquid water content to activate the CDNC, which determine the LWP.

The theoretical back ground of the above mentioned parameters with aerosols activation including condensation and evaporation schemes are explained in chapter two. The model and experimental set up are explained in chapter three, where as chapter four holds the experimental results, comparison of the results to other recent studies as well as the discussion for the intra model difference in results. Chapter five presents the results for the perturbation experiments, and chapter six closes the study with the summery of the findings and final comments.

CHAPTER TWO
THEORY

2.1 Theoretical Background

The influence of the aerosols on clouds and climate can be explained by analyzing the microphysical and radiative properties of aerosol on clouds. As explained above the sulphate aerosols injected in cloud are efficient CCN, they are expected to be associated with significant changes in CDNC as well as cloud droplet effective radius causing the change in liquid water path. This will influence the changes in short wave cloud forcing (SWCF) at the top of atmosphere for a given simulation mode of liquid water content (LWC).

The magnitude of the effect is largely dependent on the amount of the CDNC or the CCN which in great extent modifies both the microphysical and radiative parameter of cloud, Hoose et al., 2009 found that constraining of the CDNC reduces the simulated aerosol indirect effect by up to 80%. This can be done by lower or upper bounding of the CDNC as evidenced by Jones at al., 2001, Lohmann et al., 1999, 2007, Wang and Penner (2009) EST. This implies that the above mentioned variables to be among the key parameters in estimating the effect of the sulphate emission on cloud i.e. the AIE to depend on both R_e and LWP(Storelvmo et al., 2006**).**

2.2 Governing equations of the microphysical and radiative terms

Due to the importance of the above mentioned microphysical and radiative parameters it is worthwhile to explain the theoretical back ground behind these parameters. The radiative characteristics in any size distribution is represented by effective radius (R_e) which is defined as the ratio of the sum of the third and second moment of the particle size distribution (Hansen and Travis (1974)), and depends on droplet number concentration N_c and liquid water content LWC. In considering the particles concentration over a given column of air of with specified height the effective radius will be defined as in Sekiguchi et al., 2003.
Effective radius is defined as:

$$r_e = \left\langle {r^3}/{r^2} \right\rangle = \frac{\int r^3 n(r)dr}{\int r^2 n(r)dr} \qquad (1)$$

Where r is the radius of the cloud droplet, and n(r) is the cloud droplet number per unit volume.
The cloud liquid water content (LWC) can be expressed as:

$$\text{LWC} = {4}/{3}\,\rho_w \pi \int_0^\infty r^3 n(r)dr = {4}/{3}\,\pi \rho_w N_c r_{v,a}{}^3 \qquad (2)$$

$$N_c = \int_0^\infty n(r)dr \qquad (3)$$

N_c is the cloud droplet number concentration
Where $r_{v,a}$ is the volume-averaged radius, and ρ_w is the density of water.

The liquid water path LWP (W) is expressed as
W =LWC x h (4)
Where h is the cloud geometrical thickness

The cloud optical thickness is expressed as:

$$\tau_c = \frac{3}{4} Q_{ext} W \frac{1}{r_e} \rho_l \quad (5)$$

Where Q_{ext} is the extinction efficiency, which is about two for wavelengths much shorter than R_e. Under the assumption of monomodal lognormal droplet number distribution as well as liquid water clouds.

The cloud albedo can be defined as the fraction of the incident solar radiation reflected to space by clouds, which depends on the drop size, liquid water content, water vapor content, thickness of the cloud and the sun's elevation. The smaller the drops associated with greater liquid water content, the greater the cloud albedo (i.e. the more the reflectivity). Theoretically the cloud albedo is a function of scattering effect where scattering asymmetry factor has to be determined (by means of two stream approximation theory) and the optical depth which depends on effective radius and cloud droplet number concentration (equation 5) with extinction efficiency. For convenience and simplicity we can also re- write equation 5 using the GCM scaling efficiency β which is also used to obtain the R_e from the mean volume radius where Rotstayn and Liu (2003) called it as spectral shape factor which describes the width of the spectral droplet size distribution

$$\tau = 2\pi r_e^2 N.H \Big/ \beta^3 \quad (6)$$

Then using the two streams for horizontal homogenous cloud expression by Lacis and Hansen 1974 we can write expression for calculating the cloud albedo (A)

$$A = \frac{\sqrt{3}(1-g)\tau}{2+\sqrt{3}(1-g)\tau} \quad (7)$$

Where g is the scattering asymmetric factor which can be given a fixed number or calculated

It is well understood that different aerosol species of the background model cloud or aerosol, as well as the ship emissions occur in sizes ranging from Aitken, accumulation and giant aerosol. Since shipping increases the aerosol number concentration in the range of accumulation mode (Lauer et al., 2007), it becomes important to consider the life cycle, the aerosol size distribution and the activation of aerosol into cloud droplet number.

These parameters are calculated by the model at all grid points by using the algorithm which is treated as mono-modal and multi-modal lognormal size distributions as well as sectional size distributions [Abdul-Razzak et al., 1998; Abdul-Razzak and Ghan, 2002]. Whereas according to Storelvmo et al., 2006 the sectional approach would be the ideal application for the aerosol size distributions. The model treats fine mode primary sulphate POM and BC particles can mix either externally (e.g. Lohmann et al., 1999a; Tegen et al., 1997) or internally with other substances with a fixed ratio of the individual components (Haywood et al., 1997b) by condensation and coagulation, whereby at high relative humidity hygroscopic particles (including sulphate, POM and sea salt etc) grow by extracting water from unsaturated water vapor in the ambient air (Kirkevaag et al., 2007; Storelvmo et al., 2006)

2.3 Microphysical source and sink terms

The parameterization of condensation and evaporation schemes are calculated in the model, where as microphysical source and sink terms are given by equation (8) derived by Rasch and Kristjansson, 1998 under assumption that cloud droplet can be lost through evaporation, precipitation, or through self- collection where as self collection term in the model is derived by Beheng (1992). The Rasch and Kristjansson scheme includes the prognostic equation for the cloud liquid water mixing ratio and is given by:

$$\frac{dq_L}{dt} = Aq_L + Cond - PWAUT - PRACW - PSACW - E \qquad (8)$$

q_L = cloud liquid water mixing ratio,

A_{qL} = transport convection and turbulence

C_{ond}= condensation of cloud liquid water

PWAUT=auto conversion of cloud droplets

PRACW=collection of cloud droplets by rain drops

PSACW=collection of cloud droplets by snow

E = evaporation of cloud water liquid phase

The precipitation term is divided into an auotoconvension term and two collection terms i.e. the liquid droplet collected by rain and that collected by the snow. The auto conversion term PWAUT is given by equation (9) as:

$$PWAUT = \left[\left(C_{l,out} q_l^2 \rho_a\right)\frac{1}{\rho w}\right].\left[\left(q_l \rho_a\right)\frac{1}{\rho_a N_l}\right]^{1/3}.H\left(r_{3l} - r_{3lc}\right) \qquad (9)$$

ρ_a= air density, ρ_w=water density, r_{3l}=mean volume radius, r_{3lc}= critical mean volume radius, and H= heaviside function {1 if $r_{3l} \geq r_{3lc}$, 0 otherwise}

Note that $C_{l,out}$ and r_{3lc} are both relatively uncertain (Kristjansson, 2002).

2.4 Continuity equation for cloud droplet number concentration

To satisfy the need for quantifying the net effect of the aerosol indirect effect (which is uncertain due to high spatial and temporal variability of the aerosol and uncertainty of the emissions data) we also employ the Storelvmo et al., 2006 continuity equation for cloud droplet number

$$dN_L/dt \, AN_L - Nucl - \frac{N_l}{q_l}(PWAUT + PRACW + PSACW + E_1) - E_2 - Self - Freez \quad (10)$$

N_L =cloud droplet number (number density (number/cm^3))

AN_L =transport (convection and turbulence)

q_L=mixing ratio for cloud water (liquid phase)

Self = rate of self collection of cloud droplets (i.e. coalescence of droplets not resulting in precipitation)

Freez = freezing of cloud droplets to form ice crystals

E_1 = evaporation of cloud droplets for RH<100%

E_2=evaporation of cloud droplets for shrinking cloud

On simulating the continuity equation the importance of each term can be observed. The nucleation term is mostly important at the lower levels, of the model that has high moisture content, with NH leading with large number of cloud droplets due to large land covered area as compared to southern, as well as high aerosol emission sources like industries (Storelvmo et al., 2007).

Precipitation and evaporation processes are important sinks for cloud droplets. Evaporation which is proportional to the loss of in cloud water and CDNC is the dominating sink term for clouds at high latitudes and have a maximum dominancy at low latitudes around 30N, where as precipitation is an important sink terms for cloud droplets especially up to 600 hPa in mid-latitude storm tracks (Storelvmo et al., 2007). The self-collection is highly noticeable at low level clouds because liquid water content is highest at low levels and decreases rapidly with height. But this is not guaranteed in tropics due to high convection rates which transports cloud water aloft.

CHAPTER THREE
METHODOLOGY

3.1 Experimental overview

In this study the main technique used to investigate the cloud ship emissions interaction is the use of the climate model called CAM3.0 or Community Atmospheric Model version 3.0. Using this model, simulations for both microphysical parameters and radiative parameters has been conducted. Sulphate column burden (SO_4) and SO_2 acts as the aerosol sources injected into the background of the model cloud, where as the Re, (AOD, COD and CA), LWP, column CDNCINT and the CDNC (at model levels 23:25 equivalent to an altitude of 0.33-1.3km at the Ocean) were investigated for a parallel simulations of data sets (without emission, Dentener emission and Dalsoren emission).

The response of these cloud parameters to both shortwave and long wave radiations were directly calculated from the model frame work, and the TOA shortwave cloud forcing (SWCF) and long wave cloud forcing (LWCF) were calculated. The AIE or the net cloud forcing was obtained by the description given by Storelvmo et al., 2006 i.e. "We define the AIE as the difference in cloud radiative forcing (CRF) at the top of the atmosphere (TOA) between the control run and the pre- industrial (PI) run. The net CRF is the sum of the shortwave and long wave component of the radiative forcing (SWCF and LWCF), respectively". Note in our study the control run is given by the simulation of the aerosol data with Dentener and Dalsoren emissions, and the PI (pre- industrial) is given by simulations of the data with no ship emissions.

The expression used by Storelvmo et al., 2006 is mathematically formulated by Jones and Slingo (1996) as explained in Taylor et al., 1997. We will present results of TOA radiative forcing *R,* in this case due to ship tracks, as a change in the TOA net forcing thus,

$$R = (SWtr - SWbck) + (LWtr - LWbck) \quad (11)$$

SW is the net TOA shortwave irradiance; LW the net TOA long wave irradiance (where downward is positive); and the subscripts ''tr'' and ''bck'' refer to the ship track and background clouds, respectively. In our study R=> Net cloud forcing, SW => SWCF at TOA, LW => LWCF at TOA, where as tr => Dentener and Dalsøren emissions and bck => emission data without ship (no shipping emission).

The model simulations were conducted both online (with aerosol effect allowed to feed back on the model meteorology) and offline (with aerosol effect on cloud microphysics and radiation not allowed to feed back to the model meteorology) Storelvmo et al., 2006. The online model outcomes were noisy and not reflecting the geographical distribution patterns

which were expected as compared to other studies. The model performed three types of simulations where as annual, seasonal and zonal averages were calculated.
Annual averages are intended to feature the global annual variations of the ship emissions effects. The seasonal averages are aimed to describe the seasonal variations of the effects, at what areas and at what time is the effect maximum and why. This was performed due to the fact that the seasonal mean aerosol concentrations have high temporal resolution as compared to annual mean for the changing meteorological conditions Kristjansson (2002). The zonal mean simulations were intended to show the latitudinal variations of the microphysical and radiative effects of the shipping emissions on clouds for different latitude zones.

3.2 Model description

The CAM- Oslo model (Community Atmospheric Model version 3.0 or CAM3.0 [Collins et al., 2006]) is the latest in the series of global atmospheric models developed by the NCAR (National Center for the Atmospheric Research), and the model component of Community Climate System Model (CCSM), which has a major role in coupled climate system. The model is based on the advancement of CAM2.0; it includes ocean, land, and sea ice modules as well as a flux coupler. The model incorporates significant improvements to the physics package e.g. the generalized cloud overlap for radiation calculations, new capabilities such as the incorporation of the thermodynamic sea ice and a number of enhancements to the implementation (e.g. clear separation between physics and dynamics).
The model runs with a horizontal spectral resolution of T42 dynamical cores with 26 vertical levels i.e. T42 (resolution of 64 latitude x128 longitude) or T42 (2.8^0 x 2.8^0 spectral grid transform) with a temporal time step of 20min.

On initializing the model runs with a spin up time < 1 day, this is to insure that at any time desirable to start it runs with the exact state of the atmosphere with some of the past processes. In addition to initial simulations, it runs with two types of continuation runs i.e. restart and branch. Restart is an exact continuation of previous simulations from its point of termination and branch run is a new case that uses the restart data for the previous simulation to begin the integration.

CAM3.0 has been extended to include a detailed aerosol module (Seland et al., 2008) and a prognostic double-moment cloud microphysics scheme (Storelvmo et al., 2006, 2007), which allows aerosol indirect effects to be calculated refer equations (8-10). The cloud droplet nucleation, and activation (source term) as a function of updraft and super saturation are calculated by assuming the framework by Storelvmo et al., 2006 (refer section 2.2 and 2.3).

3.3 Aerosol optical properties

The three intrinsic optical properties i.e. aerosol extinction (determines interaction between aerosols and radiation), single scattering albedo (determines degree of absorption versus scattering), and asymmetry parameter ((determines the degree of forward versus back ward scattering) are computed on the band structure of CAM 3.0 using Chandrasekhar weighting with spectral solar insolation. The aerosol types affected by hygroscopic growth at 80% are sulphate, sea salt, and hydrophilic organic carbon. In CAM 3.0, the actual profiles of relative humidity computed from the model state each radiation time step are used in the calculation. The optics for black and organic carbon is identical to the optics for soot and water-soluble aerosols in the Optical Properties of Aerosol and Clouds (OPAC) data set [Hess et al., 1998].

For sulphate Mie calculations are used assuming lognormal size distribution with size parameters of median radius of 0.05μm and geometric standard deviation of 2.0. For volcanic stratospheric aerosols are assumed to be comprised with 75% sulphuric acid and 25% water, with log-normal size distribution which has an effective radius of 0.426μm and a standard deviation of 1.25. The bulk formulae of Cess [1985] are used to combine the optical properties of the individual aerosol species into a single set of bulk aerosol extinctions, single-scattering albedo, and asymmetry parameters for each layer.

Calculation of aerosol shortwave effects and radiative forcing CAM 3.0 scale the masses of each aerosol species at runtime. These factors are global, time-independent constants. This provides the flexibility to consider the climate effects of an arbitrary combination of the aerosol species in the climatology. It also facilitates simulation of climates different from present-day conditions for which the only information available is the ratio of globally averaged aerosol emissions or atmospheric loadings. A mechanism to scale the carbonaceous aerosols with a time-dependent factor has been included to facilitate realistic simulations of the recent past.

3.4 Experimental set up

The experimental procedures were performed based on the following steps

1 Conducting the test runs where by the yearly average Dentener et al., 2006 emission data was simulated into the model by using the online mode of simulations (aerosol are allowed to influence the model dynamics which again feedback on the spatial and temporal distribution of aerosol meaning that we allow the indirect effect to feed back into the model aerosol). The results were noisy and did not reflect the patterns of the expected results.

2 Conducting simulations of the annual average Dentener emission data with the offline mode (not allowing the aerosol to feedback into the model meteorology) the results obtained here were very good without noise and provides good representation of the expected results as compared to other studies including Lauer et al., 2007 and Storelvmo et al., 2006.

3 The Dentener et al., 2006 emission was successively removed, from the model CAM3.0 and replaced by that of Dalsoren et al., 2008 emission.
4 Parallel simulations for both the Dalsoren et al., 2008; Dentener et al., 2006 and without ship emissions, the reference simulation (Lauer et al., 2007) were made under the offline mode, and the results were good and showing the same patterns as expected as from other studies.
5 Experiment to observe the change in cloud parameters per change in emission were conducted. This was done to investigate how sensitive the clean areas are with respect to change in pollution
6 As the way to explain why our results for the net cloud forcing are three times lower than that of Lauer et al., 2007, the sensitivity experiment without black carbon from fossil fuels (BC) and particle organic matter (POM) was conducted.

Note: as explained in chapter one that the study will only focus on the indirect effects (first kind and second kind) of the sulphate aerosols in clouds and climate. But the model settings explained in chapter two for calculating the CDNC equation (10) and that of LWP equations (2, 3 and 4) will result low relative and percentage contribution of LWP and will not be able to distinguish the radius effect and the life time effect i.e. the model setting can't resolve the effect of aerosol emissions on cloud life time which resulting from changes in the precipitation formation efficiency. In order to accommodate this aerosols effect on the cloud life time or precipitation efficiency, the settings adopted by J. E. Penner et al., 2006 should be adopted.

This setting includes:
(i) Changing the model horizontal resolution from 2.8^0x2.8^0 (T42) to 2.0^0x2.5^0 and the dynamical time step of 30 minutes instead of 20 minutes i.e. from the Eulerian dynamical core to Finite - Volume dynamical core.
(ii) Adopting the Khairoutdinov and Kogan (2000) formulation for the auto conversion (the rate of conversion of cloud droplets to precipitation), which is given by
$P = 1350 q_l^{2.47} N_d^{-1.79}$ where q_l is the in cloud liquid water mixing ration (kg/kg)
$N_d = A\ (m_{SO4}^{2-})^B$ where m_{SO4}^{2-} is the mass concentration of sulphate aerosol at cloud base in μgm^{-3}, A and B are empirical determined constants, where the values of A an B are obtained (from formula "A" of Boucher and Lohmann, 1995).

Note that Boucher and Lohmann, 1995 relate the aerosol concentrations to droplet number concentration. This is important as explained in section 3.3 that calculation of aerosol shortwave effects and radiative forcing in CAM 3.0 lead scale the masses of each aerosol species at run time. Introduction of this formulation will lead to the increase in LWP for the present day simulation (J.E. Penner, 2006).

(iii) Because the second model setting has influenced the increase in the liquid water path the results in AIE between the these two settings (Storelvmo et al., 2006 and J. E. Penner et al., 2006) will differ (i.e. the Penner et al., 2006 will yield large changes), the relative and the percentage difference between these two results will represent the absolute and percentage contribution of life time effect in the aerosols indirect effect. This has been caused by the difference in CCN and hence difference in CDNC between the two separate runs of different auto conversion rate schemes.
(iv) It should be noted that in these three clouds water fields (schemes), one will be for advancing the model, and the other two will be for diagnostic purposes. Two changes of liquid water schemes should be for the no shipping emission and the last one should be for the inventory containing shipping emissions (Kristjansson et al., 2002).

CHAPTER FOUR

RESULTS OF ANALYZED CLOUD PARAMETERS

4.0 Lay out of the results and discussion

This chapter will be concerned with the presentation and interpretation of the analyzed simulation results reasoning and navigating to other studies for the comparison point of view. Model simulation results for both cloud parameters, for the runs with and without BC and POM have been be presented.

Note: Appendix A contains map sections which have names of some places mentioned in this study, the reader is advised to look it in order to be familiar with shipping routes and areas.

The results of ship induced effects on clouds has been based on emissions by Dentener et al., 2006, whose emission estimates are based on fuel consumption statistics with SO_2 emission total of $7.8Tgy^{-1}$ and Dalsoren et al., 2008 which have emission estimates of $4.7Tg(S)y^{-1}$). We have used two emission inventories in order to address the uncertainty due to different methods and considerations used to collect the emission data (Eyring et al., 2009; Lauer et al., 2007 and Enderson et al., 2003), leading to the uncertainty of aerosol indirect effect (AIE) which is fueled by limitations to adequately represent aerosol amount, aerosol properties and aerosol interactions (e.g. the aerosol impact on cloud properties) in global modeling.

4.1 Sulphur emission (SO_2)

Sulphur dioxide (SO_2) which is the source of sulphate burden through the oxidation by the hydroxyl radical (OH) in the gas phase or O_3 and hydrogen peroxide in the aqueous phase of cloud droplet (Lauer et al., 2007), was simulated both for the annual and seasonal conditions. The results apart of showing increasing of the SO_2 emission level due to increased shipping traffic, it also supports other studies including that of Lauer et al., 2007, Eyring et al., 2009) that Northern hemisphere(NH) have more been affected by shipping traffic than Southern Hemisphere (SH).

The model (CAM3.0) calculated global annual average SO_2 emission due to Dentener shipping is $7.49Tgy^{-1}$ with the increase of 5.8%, this compares well with both the AeroCom data ($7.8Tgy^{-1}$ or $3.8Tg(S)y^{-1}$), and $7.6Tgy^{-1}$ calculated by the E5/M1-MADE using the same emission data. For the Dalsoren et al., 2008 emission the model (CAM3.0) calculated global average for the shipping is $9.38Tgy^{-1}$ or $4.65Tg(S)y^{-1}$ with an increase of 7.2% of the back ground or (pre- industrial value). This model result of $4.65Tg(S)y^{-1}$ compares well with the $4.7Tg(S)y^{-1}$ calculated by the Chemical Transports Model (CTM) model. The model calculated difference in shipping contribution between these two emissions inventories is $1.89Tgy^{-1}$ which is about 25.23% of the global mean for Dentener et al., 2006 emission.

This percentage increase of the sulphur emission (SO_2) due to increased number of ship traffic has caused the doubling of the global average AIE due shipping emission and perturbing clean areas like the West coast of North America (Tehuantepec Bay and Californian Gulf) and areas having lower boundary marine liquid water clouds (Low stratus, stratocumulus) including the coast of North East Asia and South Western coast of Africa (Namibia and Durban) to be very sensitive to this emission change see figures 13(a-c).

The geographical distribution for the annual average sulphur emission figure (1a) have distinct peaks on the Northern Atlantic in the areas including Gulf of Mexico, Baltic Sea, North Sea, and the Southwestern and Western Europe at the areas of Norwegian Sea as well as northwestern Africa at the entrance of the Mediterranean channel. These areas have peaks values ranging from 2-5E (-12) $kgS/m^2/s$, where the highest values (level) of emission is found on the North Sea and Baltic Sea. Over the Indian Ocean the areas including the North East Asia and Gulf of Aden are characterized by the increase of up to 2 and 3.5E(-12)$kgS/m^2/s$. Apart from the dense ship traffic areas, more low density traffic areas in Atlantic, Pacific and Indian Oceans are characterized by the increase of up to 1E (-12) $kg/m^2/s$.

Due to its increased coverage, which was caused by increased ship traffic, the figures support our argument that the Dalsoren et al., 2008 emission has increased the forcing not only to Europe and America but also to Asia and Africa. On comparing the two simulation results one will find that figure 1(a) is intense in some area, but with wide coverage than figure 1(b) which is intense and covers only the main shipping routes as agreed by (Lauer et al., 2007; Dalsoren et al., 2008).

The shipping emission has increase its effect on 0S to 40S and 30N to 80N (see figure 2(a)) causing the increase in LWP and reduction in R_e due to increased CDNC caused by oxidation of sulphur dioxide to sulphate which acts as good CCN. This is well supported by the findings of our study that over the SH shipping contribute to $0.442Tgy^{-1}$ and $1.62Tgy^{-1}$ equivalent to 6% and 17% (see table 1(a)). But also the recent studies by Skjolsvik et al., 2000; Endresen et al., 2003; Corbett and Kohler, 2003 and Wang et al., 2007 come up with the report that the majority of the ship emissions occur in NH, where by estimates show that 80% of the traffic are in NH and 20% of the traffic in the SH Eyring et al., 2009.

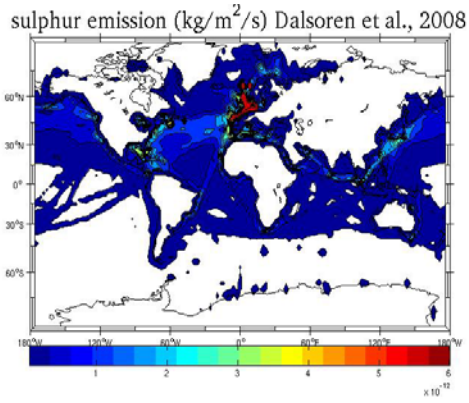

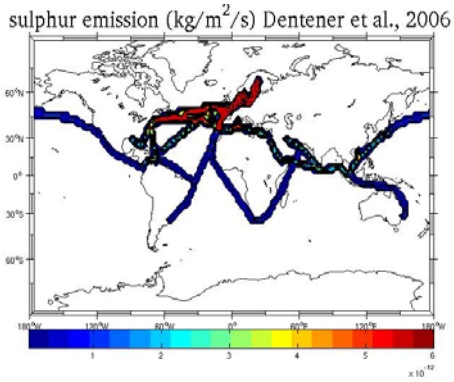

Figure 1(a) Figure 1(b)

Figures 1(a & b) annual shipping contribution for sulphur emission due to Dalsoren et al., 2008; and Dentener et al., 2006. Note the dark blue color has values ranging from 0.05≤x< 1E (-12) kgS/m^2/s and white areas have values less then 0.05E (-12) kgS/m^2/s

On the aspect of seasonality, unlike the Dentener emission which has not been subjected to the seasonal changes of SO_2, the Dalsoren emission has slight seasonal variations. These variations are more pronounced on the NH and in Northern Atlantic Ocean than SH and Southern Atlantic or Pacific Ocean. This seasonality for the Dalsoren emission is slightly shown over the JJA period (figures are not included) which is characterized by higher ship emissions. The only weak changes in its geographical distribution are observed at Greenland, Canada, Arctic Sea as well as Northern areas of North America.

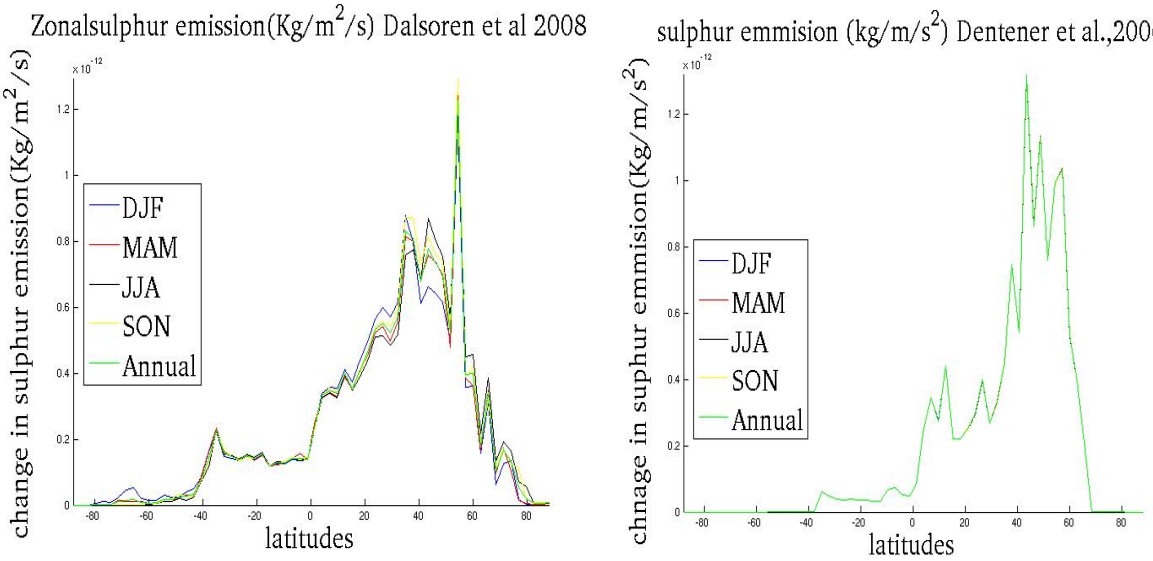

Figure 2(a &b) the zonal variation of sulphur emission for Dalsoren and Dentener shipping emissions

In zonal aspect figure 2(a) show that there is an increased amount of sulphur emission of up to $0.23x10^{-12}$ kgS/m^2/s in the Southern latitudes ranging from 0 to 40S. Also at high latitudes

60S and 80S for the SH summer period (DJF) seasonal period the figure 2(a) has shown an increase in traffics over this latitude zone.

4.2.1 Sulphate burden

AIE which exhibits large geographical variation is not only due to change in aerosol amount or burden in the atmosphere, but also other factors including surface albedo, solar zenith angle, cloud height est.(Kristjansson et al., 2002). As far as emissions are concerned the sign of the AIE is very dependent on the type of emissions under consideration (i.e. it is positive for the CO_2 and negative for sulphate). This excessive aerosol loading alters the properties of the cloud and hence the AIE (Storelvmo et al., 2006).

The global geographical distribution of the sulphate column burden and how it maps in the atmosphere near the ground surface is as shown by figure 3(a-d), where all figures support the fact approved by many studies that the effect of the anthropogenic ship emissions is more significant in the NH than in the SH (Storelvmo et al., 2006; Lauer et al., 2007; Eying et al., 2009). With figure3(a) having the highest peak of up to 2.5kgS/m^2 at areas of Baltic sea and North Sea, as supported by (Derwent et al., 2005), who has found that North Sea and Baltic Sea contribute to about 50% of the total sulphate deposition which occurs over Europe, where as along the western coasts of the UK and Scandinavia, contribute to about 10% and 25% of total sulphur deposition from shipping (Dore et al., 2006; Dalsoren et al., 2007; Collins et al., 2009)).

Sub peaks which are characterized by a change of up to 1.5kgS/m^2 occur at Northern Atlantic Ocean in areas including Gulf of Mexico, North West Africa at the entrance to Mediterranean Sea, boarded by Portugal and Spain for Europe and Morocco for Africa, the English Channel and Gulf of Biscay. The remaining ship traffic areas are influenced by the change ranging between 0.1 to 0.5kgS/m^2.

The figure also show that there is an annual increase of the ship traffic from Southern part of North America to Europe as well as to NW part of Africa (Northern Atlantic Ocean).
Comparatively figure3 (a) has more emission effect (wide coverage with little strength) than figure 3(b) which has only high strength. Figure 3(b) has only the strong highest peak ranging from 3.5E(-7) to 4E(-7) kgS/m^2 over the areas of the Baltic Sea, North Sea, where other areas including the English Channel, the South Western coast of Norway are characterized by a change of 2E(-7) to 2.5E(-7) kgS/m^2. Both figures 3(a & b) have highest changes over the Northern Atlantic.

Figure 3(a)

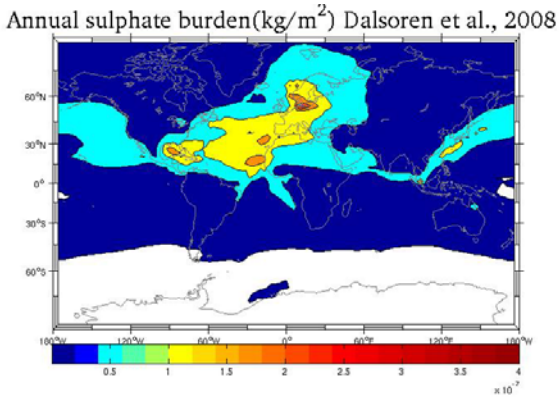

Figure 3(b)

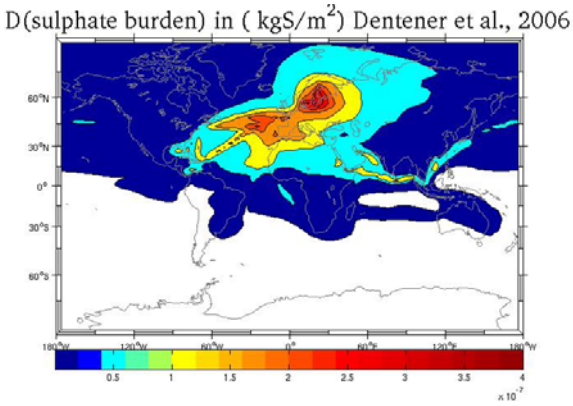

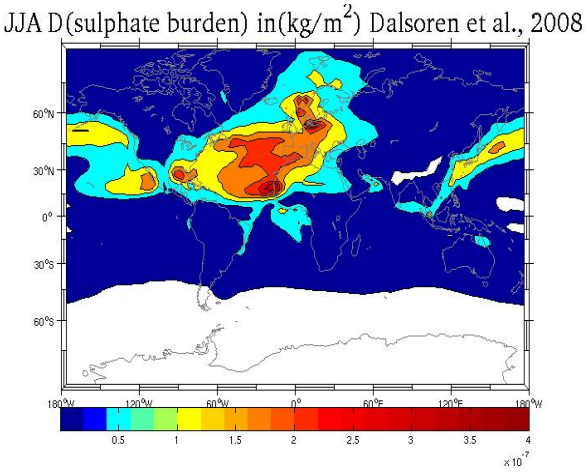

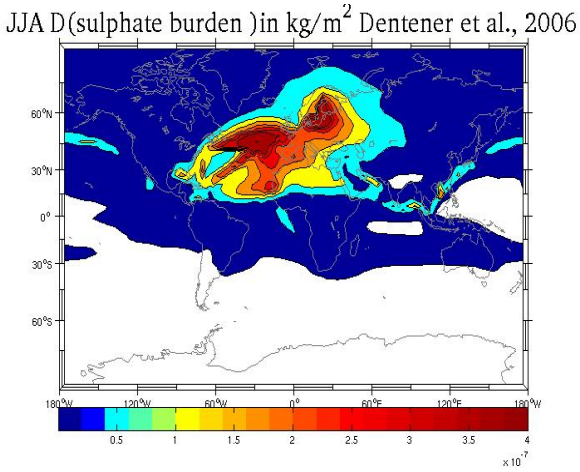

Figure 3(c) Figure 3(d)

Figure3 (a-d) the geographical distribution of the global annual and seasonal ship induced sulphate burden in kgS/m^2. Figures 3(a & c)) are the global annual and seasonal (JJA) shipping contribution due Dalsoren shipping emission. Figures 3(b & d) are the global annual and seasonal (JJA) shipping contribution due to Dentener shipping emission. Note in the color bar the blue color has values ranging from 0.1 ≤x< 0.5E (-7) kgS/m^2 where as the white areas are less than 0.1E (-7) kgS/m^2

The model (CAM3.0) calculated annual global average for total atmospheric sulphate burden is 1.76Tg with the shipping contribution of 0.051Tg or 3.0% and 1.77Tg with the shipping contribution of 0.0655Tg or 3.8% of the total atmospheric sulphate burden depending upon the inventory. When compared to total atmospheric sulphate burden of 1.511Tg with shipping contribution of about 2.3%, calculated by E5/M1-MADE using the same emission, you will notice that CAM3.0 result is slight high by 0.249Tg, also its percentage shipping contribution of 3.0% is higher than 2.3% calculated by E5/M1-MADE. This can be best explained by the intra model difference in chemistry and vertical transport in the marine boundary layer (MBL) (i.e. the intra model difference in the gaseous and aqueous oxidation of SO_2 to sulphate particle and the distraction of methane and ozone (O_3) by OH radical).

In view of both hemispheres, and as means of supporting the argument that NH is more affected than the SH, the model simulations for SH were conducted, and the results for the total SH atmospheric sulphate burden are 0.507Tg and 0.716Tg depending on the inventory. The shipping contribution is 0.0067Tg and 0.0158Tg, which are about 7% and 12% (refer table 1) of the global mean ship induced sulphate burden. This implies that ship traffic to and from SH has been increased to a significant extent, such that we can't any more say that it is still pristine.

Apart from annual mean, the seasonal and zonal variations were calculated, where by figures 3(c & d) above are the geographical distribution of the ship induced sulphate burden for the JJA. We have chosen this season because it has caused the highest net radiative forcing and putting all other parameters like LWP, R_e and sulphate burden est. at high values. The reasons why this season has high values are explained in section 4.6.1.

Figure 3(c and d) reveals that there is an increased traffic which has caused an increase in both the strength and coverage of the sulphate burden over the Northern Pacific Ocean in regions such as West of North America at Tehuantepec Bay near Santa Cruz and Californian Gulf (figure 1(c)). Over Northern Atlantic Ocean the highest peak has been marked over the same areas but more in strength, where as an increase in coverage has mapped over the Norwegian Sea, the Arctic Sea and Svalbard.

There is a marked increase in the traffic over North East Asia of up to $1.5x10^{-7}kgS/m^2$ where as areas at Southern Asia also has shown the significant increase in burden as supported by (Eyring et al., 2009). Further reflections reveal the slight North ward shift of the shipping effect over this period of the year implying that ship traffic is more concentrated at the NH.

4.2.2 Zonal distribution of sulphate burden

Figure 4(a - b) represents the results of the ship induced sulphate burden on latitudinal (zonal) distribution. Both of these plots support the findings that there is a higher level of polluting the atmosphere by ship traffic at the NH than in the SH, with 20^0N to 60^0N latitude areas being leading. Also both plots support that JJA seasonal period is the highest as supported by black peaks for both figures.

An interesting feature is that obtained from the summer period (see figure 4(a)) that there are three distinct peaks of ship induced sulphate burden one at 40^0N-60^0N, and other two at 20^0N and 20^0S showing that not only in NH that cloud raditiave and microphysical effect due to shipping emission is observed but also over the SH low latitudes or (tropical to subtropical regions) over both Atlantic and Pacific Ocean.

Apart from the seasonal mean the annual global mean (green in color) is also peaked over the NH with a significant peak at 0 to 60^0N and 0 to 40^0S, showing that the increase in ship traffic has enhanced the increase in sulphate burden from 7% to 12%. Figure 4(a) show the distinctive features of an increased sulphate burden at high southern latitudes (60S to 80S) during the DJF. This can be explained by the traffic which goes to and from Antarctica to have peak at this period of the year as agreed by (Dalsoren et al., 2008; Shirsat and Graf, 2009).

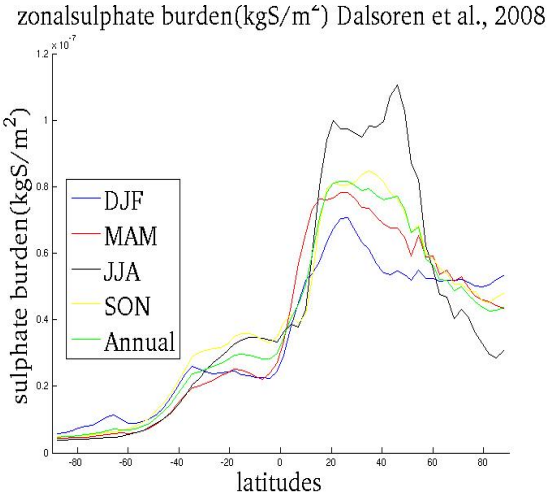

Figure 4(a)

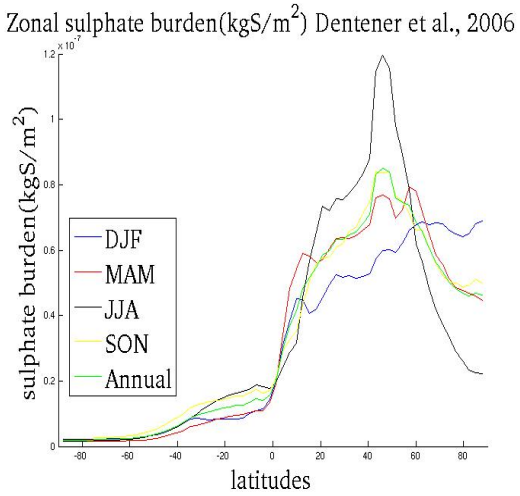

Figure 4(b)

Figures 4 (a & b) the annual and seasonal zonal mean ship induced sulphate burden;

Table (1a) the annual and seasonal changes in sulphur emission (Tgy^{-1}) and sulphate burden (Tg) globally, JJA and the Southern Hemisphere for the Dalsoren and Dentener emission inventories

variable	$(So2)Tgy^{-1}$	$\Delta(So2)Tgy^{-1}$	% Δ (So2)	(So4)Tg	Δ(So4)Tg	% Δ(So4)
Dentener	1.37e(+2)	7.49	6	1.76	0.051	3.0
Dalsoren	1.39e(+2)	9.38	7	1.77	0.0655	3.8
	The global changes for (JJA) or NH summer period					
Dentener	35	1.89	25	2.05	0.0572	28
Dalsoren	35	2.35	25	2.07	0.0736	28
	The changes on the Southern Hemisphere					
Dentener	20	0.442	6	0.507	0.0067	7
Dalsoren	21	1.62	17	0.716	0.0158	12

Table (1a) is the summarized results of the annual, seasonal as well as the SH ship induced SO_2 and sulphate burden in (Tgy^{-1}, Tg and $Tgss^{-1}$ => (Tg/season) for the JJA season). Note that the % contribution of the JJA and SH are relative to the global annual mean contribution.

Table (1b) the seasonal changes in the sulphur emission ($Tgss^{-1}$ =>(Tg/season)) and sulphate burden (Tg) for December, January, February(DJF), March, April, May (MAM),and September, October, November (SON) and their % shipping contribution relative to annual mean for Dalsoren and Dentener emission inventories

variable	$(So2)Tgss^{-1}$	$\Delta(So2)Tgss^{-1}$	% Δ (So2)	(So4)Tg	Δ(So4)Tg	% Δ(So4)
	The seasonal changes for December, January, February (DJF)					
Dentener	34.0	1.85	25	1.48	0.0441	22
Dalsoren	34.4	2.30	25	1.50	0.0569	22
	The seasonal changes for March, April, May (MAM)					
Dentener	34	1.89	25	1.66	0.0505	25
Dalsoren	35	2.34	25	1.67	0.0627	24
	The seasonal changes for September, October November (SON)					
Dentener	34	1.79	24	1.83	0.0522	26
Dalsoren	35	2.32	25	1.85	0.0689	26

4.3.1Aerosol Optical Depth (AOD); Cloud Optical Depth (COD) and Cloud Albedo (CA)

The aerosol optical depth is highly depends on the spectral parameter (wavelength), different wavelengths will result different values of the optical depth. The cloud parameters including AOD, COD and CA, R_e est. are related to each other as agreed by Schwartz et al., 2001 who reported fairly strong spatial correlations of monthly mean AOD and number concentration with R_e (negative correlation) and COD (positive correlation). Also K. Kawamoto et al., 2004 has shown that as AOD increases due to increased sulphur emission, R_e decreases. Both results (Schwartz et al., 2001 and K. Kawamoto et al., 2004) are consistent with Twomey conclusion. Equations (5) and (6) provides the relation between COD and CA also the relation is agreed by (Eyring et al., 2009) that the brightness of a cloud or cloud reflectivity (CA) observed from space is determined primarily by its visible optical thickness (COD), which is potentially increased by perturbation of a cloud layer by ship-generated aerosols.

Since for the fixed water content CDNC and COD are inversely relate with R_e equations 3 and 5, the findings by Twomey et al., 1968; Durkee et al., 2000c; Schwartz et al., 2001*;* K. Kawamoto et al., 2004; Lauer et al., 2007 and Eyring et al., 2009 will cause the slight increase in the LWP, enhancing the decrease in the R_e of cloud droplets, leading to the increase of COD and hence enhance the CA.

The annual and seasonal average AOD at optical wavelength of 550nm, COD and CA (using equation (5) and (6) for $Q_{ext} = 2$ and $g = 0.85$ for short wave length range (visible range)) was calculated for all grid points, where the results for COD and CA are presented in geographical distribution contexts and that of AOD is zonal presented.
Figure 5(a-b) are geographical distribution results for the model simulated ship induced annual COD and CA from Dalsoren inventory.

Figure 5(a)
ship induced cloud optical depth dalsore et al., 2008

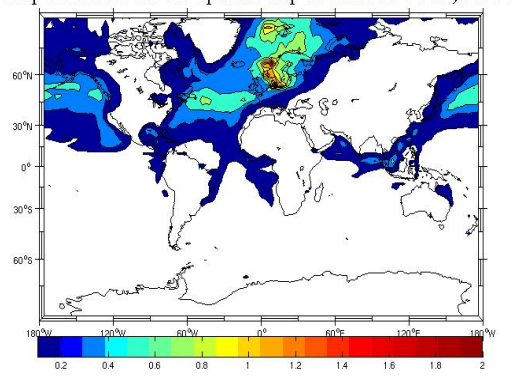

Figure 5(b)
ship induced albedo Dalsoren et al., 2008

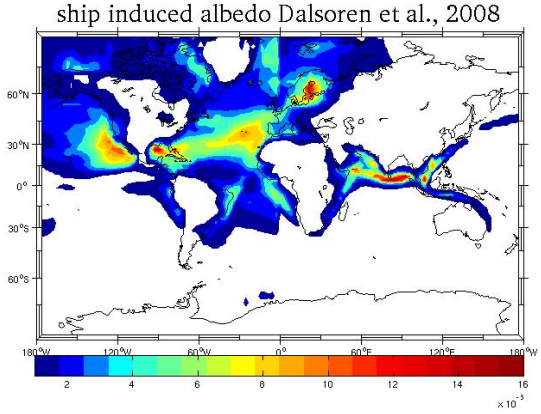

Figures 5(a-b) annual ship induced cloud optical depth (COD) and cloud albedo (CA) due to Dalsoren et al., 2008 Note the dark blue color in the figure5(a) has values defined by 0.1 ≤x< 0.2; whereas the white areas have values less than 0.1, for figure 5(b) the dark blue color has the values defined by 1 ≤x< 2x10^(-3), and the white areas are less 1x10^(-3)

Figure 5(a) resembles to the geographical distribution of near surface sulphate burden (figure3 (a)) both of them putting the more emphasis to the NH and supporting the argument of shipping emissions to have high effect on the 30N to 60N, but also the figure show that there is an increase in aerosol number concentration over the SH around 0S to 30S. The figures also support the conclusion made by Twomey conclusion that the increased optical depth is consistent with the additional CCN injected into the clouds. Thus why examination of figure 1(a) and 3(a) reveals that areas influenced by high emission and burdens matches exactly with the areas having high COD (figure 5(a)) as well as CA (figure 5(b)). Not only had the matching of peaks and sub peaked but also the coverage and strength.

For figure 5(b) the maximum values of cloud brightness are at areas with high response to SWCF, comparison of figure (5a) with figure 13(a) reveals that SWCF is mainly determined by the cloud albedo which is also a function of LWP and R_e for a given value of super saturation or LWC. Also it agrees with the relation that $\Delta N/N=\Delta R_e/ R_e =\Delta CA$ this is clearly shown by figures (7b, 7e and 9b) and agreed by Kristjansson et al., 2002.

The model calculated annual global average for AOD is 0.162 and 0.163 with the shipping contribution of 0.0013 equivalent to 0.81% and 0.00172 equivalents to 1.1% based on the inventory. These model AOD values at (550mn) are in agreement with the MODDI-MESIR (0.16) composite (Stier et al., 2005) but higher than that of Aero COM (0.127), as well as ECHAME5-HAM of 0.14 (Kinne et al., 2006; Feichter1et al., 2004). Other studies including the Krishna et al., 2004 during Arabian Sea Monsoon Experiment (ARMEX-II) campaign they found that; mean monthly AOD at 500nm wavelength over the ocean 0.44 were

comparable to those over the coastal land 0.47, but were lower than the values observed over the plateau.

In case of COD the global mean value (based on the variables in equation 5) gives the annual mean COD of 13.3792, 13.4189 and 13.3209 for the Dentener, Dalsoren and no ship emissions. This COD value is in agreement with satellite retrievals by Han et al., 1998 that for $\tau<15$, over oceans cloud albedo decreases with decreasing R_e. The ship induced value for COD is 0.0583 equivalents to 0.4% and 0.098 equivalents to 0.7% depending on the inventory. This slight increase in COD reflects the increase in the cloud brightness which is influenced by slight ship induced increase in cloud liquid water path (section 4.6.1) and decrease on R_e (section 4.5.1). For CA the annual global mean shipping contribution is 0.0008 and 0.0016 equivalent to 0.28% and 0.14% i.e. the ship induced CA for Dalsoren is twice that of Dentener.

Over the dense ship traffic areas of Pacific Ocean and Atlantic Ocean the study come up with high increase in AOD of about 0.00228 and 0.00251 for Pacific Ocean, and about **0.00311** and **0.00348** for Atlantic Ocean. These values are higher compared to the global mean values of 0.0013 and **0.00172** for the two used inventories. We have not calculate the COD and CA for these areas but we have used the existing correlation between AOD, COD and CA as given in equations (2-5) to explain an increase in cloud brightness which is caused by the decrease in R_e (due to increased CCN, K. Kawamoto et al., 2004), which will in turn induce the increase in the LWP. The results of the change in LWP in both global and regional will be presented in section 4.6.1

The seasonal global mean shipping contribution on AOD, COD and CA for the JJA show the increase in AOD by 0.00144 and 0.00197, where as the difference from the seasonal global mean to the annual global mean is 0.00014 equivalents to 2.7% and 0.00025 equivalents to 3.6% of the annual global mean. This season yields a contribution of 22% and 28% to the annual global mean AOD. For COD the season has ship induced value of 0.0721and 0.1191with the difference of 0.0211 and 0.0138 equivalent to an increase of 5% and 6%, and the contribution to the annual is 30% and 31%, where as for CA the ship induced value is 0.0010 and 0.0018 equivalent to an increase of 28% and 31% of the annual global mean CA depending on the inventory.

4.3.2 Zonal distribution of AOD

The annual and seasonal zonal averages for the AOD figures 6(a & b), reflects a clear image of induced high concentration of sulphate particles due to high oxidation rate of (SO_2) emission caused by increased ship traffic over the latitude region 30N to 80N with the peaks at around 40N to 60N. For the SH the zonal mean AOD reflects the impact of increased

emission level due international ship traffic, which has influence the ship induced AOD to increase from hemispherical annual mean of 0.00022 to 0.00064 equivalent 8.5% and 8.6% of the annual global mean AOD. This increase is found on the region between 0S to 40S, but also at higher Southern latitudes (60S to 80S) during the DJF season at the areas of Antarctic figure 6(a). Irrespective of the inventory used tropical to subtropical Oceans of NH (0N-20N) have higher contribution of ship induced AOD compared to subtropical Oceans of the SH (0S-20S)

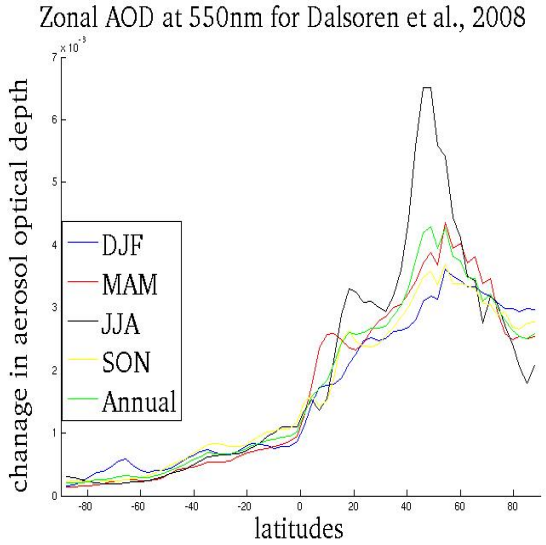

Figure 6(a)

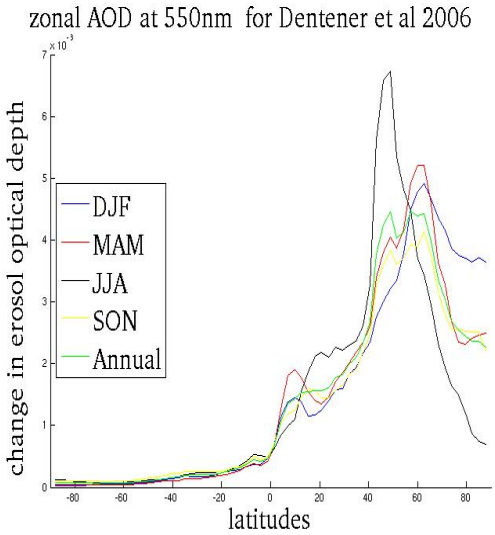

Figure 6(b)

Figures 6(a & b) the annual and seasonal zonal mean ship induced on AOD (550nm),

4.4.1 Cloud droplet number concentration (CDNC)

The simulation of CDNC as given in equation 3 (empirical formula) and equation 10 (prognostic equation) in both column and layers was performed by the model. The annual, seasonal and zonal average column CDNC was calculated by the model. For Ocean and coastal areas that are influenced by having high density of shipping (these areas are most susceptible to modification due to ship emissions), hence the CDNC and R_e at model layers 23 and 24 equivalent to average altitude of (0.69-1.3) km and levels 24 and 25 equivalent to average height of (0.33 -0.69) km were calculated for the coastal and Oceanic areas including Pacific West of North America, the Pacific West of South America, the Atlantic West of North Africa, Atlantic West of Southern Africa and the Pacific East of North East Asia.

This was not only aimed at quantifying and comparing the concentration and size of the CDNC in high ship traffic areas over Atlantic and Pacific Oceans, but also differentiating the CDNC over the coastal areas and that over the deep Ocean as concluded by Bennartz (2007), that marine boundary layer clouds even over the remote ocean have higher CDNC in NH

compared to SH (Lauer et al., 2007). In practical view of the Bennartz (2007) conclusion, the model simulations for the Pacific Ocean and Atlantic Ocean was also performed and the CDNC and R_e (at the same levels) were quantified (see tables (3(b) and 3(c))

The model calculated global mean total atmospheric column CDNC are 2.41E(+6) cm^{-2} and 2.43E(+6) cm^{-2} where the shipping contribute to 0.0258E(+6) cm^{-2} equivalent to 1.08% and 0.0446E(+6) cm^{-2} equivalent to 1.87% (see table 5) for both inventories. These model values are approximately at the same order of magnitude to the global mean total atmospheric column CDNC obtained by other studies including Storelvmo et al., 2006; the satellite retrievals by Han et al., 1998; and are same as the expected value of the CAM3.0 model as given by Gettelman et al., 2008.

The model calculated global mean CDNC for the JJA season are higher than the annual global values. Over this season shipping contribute to 0.0372E(+6) cm^{-2} and 0.0587E(+6) cm^{-2}, these values are greater by 0.0114E (+6) equivalent to 11% and 0.0141E(+6) equivalent to 8% of the global average ship induced column CDNC depending on the inventory. The contribution of this season to the annual global mean is 36% and 33% (see table 5), which indicate that JJA season contribute to approximatelly1/3 of the annual global average.
For SH the shipping contribute to 0.00683E(+6) cm^{-2} and 0.0228E(+6) cm^{-2} equivalent to 26% and 13% of the annual global mean CDNC, implying that the shipping traffic over this area has resulted the increase (not in size but in number concentration) of column CDNC.
This growth is in agreement with the zonal distribution of column CDNC figure 8(a) as well the percentage contribution to the global mean column CDNC (refer table 5).

The ship induced column CDNC for (figure 7(a)) show the wide coverage and distributed maxima and sub maxima over the Northern Atlantic in areas of South eastern America (Gulf of Mexico), Baltic sea, southwestern Europe (in areas including the Spain Portugal as well as the English Channel) and in the areas of North western Europe. These maxima or peaks has column CDNC of up 2.5E(+5) cm^{-2}. Areas of Pacific west coast of North America (Californian Gulf) as well as the coast of North Eastern Asia, west coast of southern Africa and the east coast of Australia has been subjected with a change of up to (0.5-1)E(+5) cm^{-2}.

The % column CDNC figure 7(b) has not only mapped the high ship traffic areas, but also clean areas that are susceptible to emission change causing the increase in percentage change in column CDNC. This figure has a peak percentage change of up to 10% in the Northern Atlantic Ocean, also on areas of Pacific western coast of North America, and most of areas which are characterizes by low marine boundary layer liquid water clouds have shown to be susceptible with the change in emission (sulphate particles), and hence increase in percentage change in column CDNC. A sensitive case in this figure is the areas in Baltic Sea and Northern Sea which have shown a high increase in column CDNC but also the highest

increase in percentage change in column CDNC, indicating that either the area is not highly polluted or CAM3.0 has low background cloud CDNC (refer table 2(a)). Note that this mentioned area has been reported to be sensitive to various ship emission inventories such as Dentener et al., 2006; Wang et al., 2007 and Dalsoren et al., 2008; and various studies including Lauer et al., 2007; Eyring at al., 2009.

In figure 7(c)) ship induced CDNC is mostly confined on main shipping route over Northern Atlantic Ocean, and being characterized with little coverage but high intensity of change in CDNC of up to 4.0E (+5) cm^{-2} in the areas of Baltic Sea, followed by sub maxima of (2.5 - 3.5)E(+5)cm^{-2} in the Atlantic Ocean, where as other areas are mainly subjected to a change of (0.5 - 1.5)E(+5) cm^{-2}. The percentage change of CDNC for (figure 7(d)) has mapped the great change over the Northern Atlantic Ocean of up to 25% in the Baltic Sea and North Sea, where as areas of south western Europe where the dense ship traffic occurs have been subjected to a change of up to 20%. Southern Atlantic, Pacific Northwest of North America, North East Asia est. has been subjected to little percentage change of up to 5%. Areas of western Greenland which has shown to have very little change CDNC has been subjected to a high percentage change of 8-10%, indicating that the area is more susceptible to changes i.e. due to its low back ground perturbation of ($\Delta N/N$) has agreed with findings of Taylor et al., 1997; Sekiguchi et al., 2003.

Figure7(a)

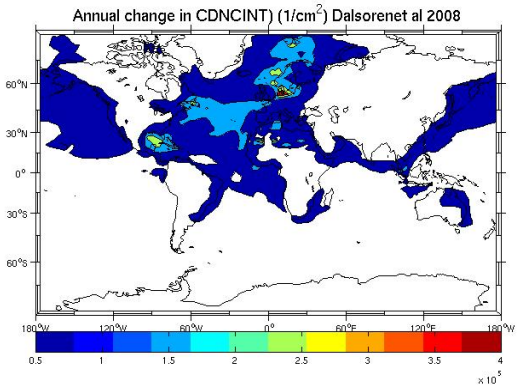

Figure7(c)

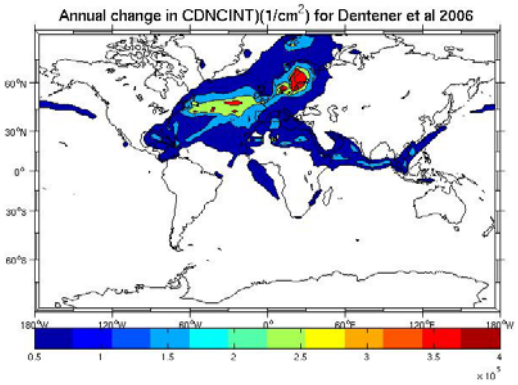

Figure 7(b)

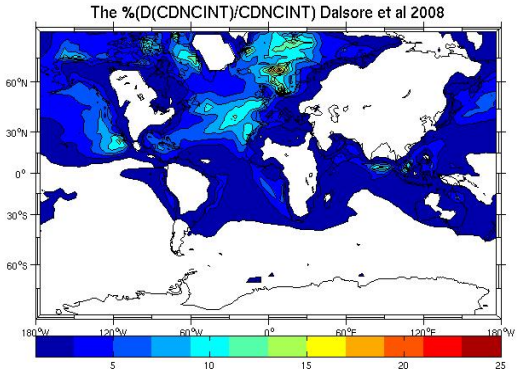

Figure 7(d)

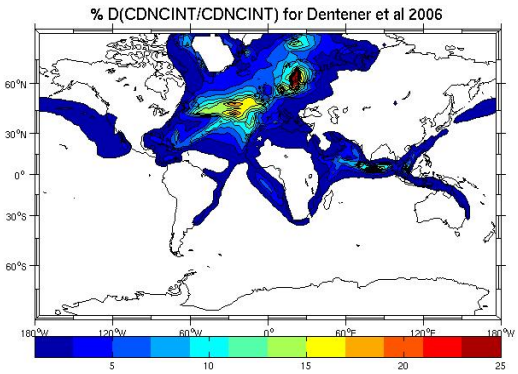

Figure 7(e)

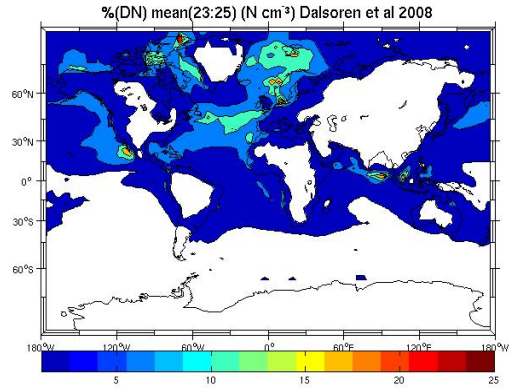

Figure 7(f)

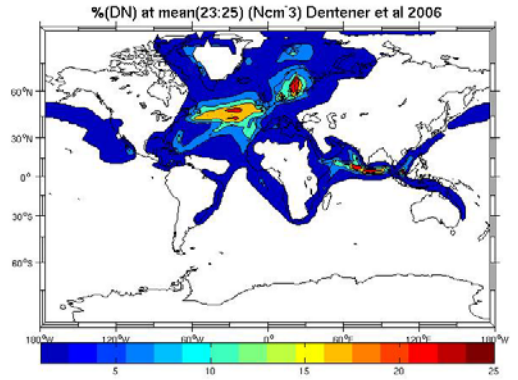

Figures (7(a &b)) are the relative and percentage change in column CDNC (Ncm^{-2}) or (ΔN_c) and $\%(\Delta N_c)$ for Dalsoren et al., 2008; Figures 7((c & d)) are the relative and percentage change in column CDNC (Ncm^{-2}) or (ΔN_c) and $\%(\Delta N_c)$ for Dentener et al., 2006; Figures 7(e & f) are the percentage changes in CDNC $\%(\Delta N)$ with the model level 23:25 equivalent to altitude of (0.33-1.3km) for Dalsoren and Dentener emission.

For the ship induced effects of lower troposphere, at an average altitude of about (0.33-1.3) km, equivalent to CAM3.0 (level 23:25 over ocean), the annual average change in CDNC was simulated, where by figures 7(e &f) represents the annual average percentage changes.

The results show that the highest percentage change of roundabout (8-9)cm^{-3} equivalent to (10-15% Dalsoren emission) and (8-20% Dentener shipping emission) occurs over both the Pacific and the Northern Atlantic in the areas which are characterized by the low liquid water marine clouds. These areas include Northwestern part of Africa, southwestern Europe at the entrance of Mediterranean Sea bordered by Portugal, Spain and Morocco. Over the Mediterranean Sea, Suez canal, Southwestern coast of Africa, Australia, Red Sea and South East to North East Asia CDNC has risen up to (2-4) cm^{-3} equivalent to 2-10% and 2-14%, where as Gulf of Aden the increase has been up to 6cm^{-3} equivalent to 15-20% and 15-25% based on the inventory.

From these results we can conclude that the Dalsoren emission inventory has been very sensitive to the change of cloud droplet number concentration over areas with less frequent shipping traffics, where as the Dentener emission inventory has been less sensitive to these areas, also all inventories are more sensitive to changes in cloud droplet number concentration at low model levels than at higher levels.

Based on the sensitivity and impact shown by changes in CDNC (figure 7e-7f), on lower boundary marine liquid water clouds, further analysis has been done on quantifying the exact changes of CDNC over the specific areas which has shown high sensitivity due to increased CCN.

Table (2a) Annual average CDNC (Ncm^{-3}) and $R_e(\mu m)$ calculated by CAM3.0 for the low marine clouds (0.69-1.3km) equivalent to model levels (23 and 24). Number in parenthesis are results from the E5/M1-MADE for the model level 16(0.61-1.1km) refer table 2 page 5068 of Lauer et al., 2007 paper.

Region	Dalsoren	Dentener	No ship
North America (155W-105W,18N 39N)	N=53.21 R_e=13.15	N=51.47(119) R_e=13.29(10.68)	N=50.94(118) R_e=13.33(10.73)
North Africa (45W-10W,15N-45N)	N=58.11 R_e=13.19	N=57.8(129) R_e=13.22(10.24)	N=54.70(118) R_e=13.44(10.39)
South America (100W-60W,37S-8S)	N=34.66 R_e=15.14	N=34.25(98) R_e=15.18(11.70)	N=34.22(98) R_e=15.18(11.70)
South Africa (20W-20E,30S-0S)	N=46.24 R_e=14.47	N=45.49(116) R_e=14.54(11.81)	N=44.80(114) R_e=14.60(11.82)
Northeast Asia (110E-170E,16N-35N)	N=78.14 R_e=12.65	N=77.26(115) R_e =12.72(8.58)	N=76.77(114) R_e =12.74(8.59)

Table (2b) annual average ship induced CDNC (ΔNcm^{-3}) and R_e ($\Delta R_e\mu m$) calculated by CAM3.0 for the marine low clouds (0.69-1.3km) equivalent to model levels (23 and 24) numbers in parenthesis. And model levels 24 and 25 equivalent to average height of (0.33-0.69km) the first numbers, for the grid box areas defined in table (2a). The numbers in bold are from E5/M1-MADE calculations for the model level 16(0.61-1.1km).

region	Dalsoren		Dentener	
	$\Delta N(cm^{-3})$	$\Delta(R_e\mu m)$	$\Delta N(cm^{-3})$	$\Delta R_e(\mu m)$
North America	4.16(2.27)	-0.27(-0.18)	0.9(0.54)(**1**)	-0.06(-0.04)(**-0.05**)
North Africa	5.59(3.41)	-0.29(-0.25)	5.02(3.10)(**11**)	-0.25(-0.22)(**-0.15**)
South America	0.64(0.44)	-0.05(0.04)	0.02(0.02)(**0**)	-0.0015(0.0025)(**0**)
South Africa	2.17(1.44)	-0.129(-0.125)	0.97(0.69)(**2**)	-0.061(0.056)(**-0.01**)
North EAsia	1.82(1.38)	-0.132(-0.093)	0.64(0.50)(**1**)	-0.039(-0.024)(**-0.01**)

Table (3a) annual average percentage (%) shipping contribution (%ΔN) and (%ΔR_e) calculated by CAM3.0 for the marine low clouds (0.69-1.3km) or model levels (23– 24) numbers in parenthesis. Model levels (24-25) or (0.33-0.69km) the first numbers, for grid boxes defined in table (2a). The numbers in bold are from E5/M1-MADE results for model level 16(0.61-1.1km), Lauer et al., 2007.

region	Dalsoren		Dentener	
	%ΔN	%ΔR_e	%ΔN	%ΔR_e
North America	6.66(4.46)	-2.05(-1.38)	1.44(1.05)(**0.53**)	-0.46(-0.33)(**-0.465**)
North Africa	7.14(6.23)	-2.22(-1.84)	6.41(5.6)(**9.32**)	-1.91.(-1.61)(**-1.44**)
South America	3.44(3.21)	-0.32(-0.20)	0.04(0.07)(**0**)	-0.0098(-0.016)(**0**)
South Africa	2.17(1.44)	-0. 92 (-0.86)	1.543(1.540)(**1.75**)	-0.396(0.414)(**-0.085**)
North EAsia	2.42(1.79)	-1.06(0.73)	0.858(0.648)(**0.88**)	-0.308(-0.184)(**-0.116**)

Table (3b) Annual average ship induced changes on ($\Delta N cm^{-3}$) and ($\Delta R_e \mu m$) over Pacific and Atlantic Oceans the changes are for model level (24- 25) or (0.33-0.69km) which shows the maximum sensitivity due to shipping. The numbers in parentheses are given for model level (23 – 24) or (0.69-1.3km). The bolded numbers are for E5/M1-MADE results for model levels 17(0.3-0.6km) and 16(0.6-1.1km) refer table 5 in Lauer et al., 2007.

Region	Dalsoren		Dentener	
	ΔCDNC(cm^{-3})	ΔR_e(μm)	ΔCDNC(cm^{-3})	ΔR_e(μm)
Pacific ocean 120E -80W 40S-60N	2.414(1.657)	-0.148(-0.126)	1.951(1.377) **13.7(4.2)**	-0.268(-0.254) **-0.15(-0.03)**
Atlantic ocean 75W-15E 40S-60N	3.244(2.22)	-0.182(-0.156)	2.547(1.711) **15.5(5.1)**	-0.141(-0.126) **-0.17(-0.04)**
Global mean	1.15(1.03)	-0.108 (0.088)	0.879(0.167) **5.9(1.8)**	-0.055(0.050**)** **-0.06(-0.02**)

Table (3c) percentage changes (%ΔN) and (%ΔR_e) due to shipping .The numbers are given in model level (24-25) or (0.33-0.69km) over ocean, which shows the maximum sensitivity due to shipping. The values in parentheses are for model level (23-24) or (0.69-1.3km) over ocean. Bolded number is from E5/M1-MADE results.

Region	Dalsoren		Dentener	
	%ΔN	%ΔR_e	%ΔN	%ΔR_e
Pacific ocean (120E -80W 40S-60N)	3.61(3.02)	-1.16(-0.93)	2.92(2.51) **5-10**	-2.10(-1.88)
Atlantic ocean (75W-15E 40S-60N)	4.70(3.96)	-1.42(-1.15)	3.69(3.19) **20-30**	-1.098(-0.929)
Global mean	2.78(2.40)	-0.83 (-0.62)	1.58(1.43)	-0.422(0.352**)**

Observations from tables 2 - 3 lead to the following key points.
(i) Low marine boundary layer cloud over the NH has more CDNC than the SH (Bennartz, 2007). Examples are the Atlantic west of North Africa (55-58 cm^{-3}), while the Atlantic west of South Africa (45-46 cm^{-3}) the difference (ΔN) of $3cm^{-3}$ for both inventories over Atlantic west of North Africa, but $1cm^{-3}$ for only Dalsoren over the Atlantic west of South Africa. The same effect holds between the Pacific west of North America (51-$53cm^{-3}$) and Pacific west of South America (34-$35cm^{-3}$) with ΔN of 2 cm^{-3} for Dalsoren and less than $1cm^{-3}$ for Dentener (See tables (2 to 3)). With the same places but with model level 24:25 (0.33-0.69)km, the Atlantic west of North Africa has the ΔN of $5cm^{-3}$ for both inventories, whereas over the Atlantic west of south Africa the changes has been only $2cm^{-3}$ and less than $1cm^{-3}$. Over the Pacific west of North America the difference has been $4cm^{-3}$ and approximately $1cm^{-3}$, where as for the Pacific west of South America the difference is very small, indicating less frequent shipping traffic over this area.

(ii) The model levels (23:24 and 24:25) (over the Ocean) for Atlantic Ocean has more CDNC than Pacific Ocean. At model level (23:24), ΔN of 3 cm^{-3} is higher in Atlantic west of North Africa for all inventories, than ΔN of $2cm^{-3}$ and ΔN of $1cm^{-3}$ for (Dalsoren for Dentener) in the Pacific west of North America. The same case applies to the Atlantic west of South Africa, and Pacific west of South America (refer tables (2 to 3)). For the model levels 24:25, the Atlantic north of west Africa has ΔN of $5cm^{-3}$ for both inventories, which is higher than ΔN of $4cm^{-3}$ and ΔN of $1cm^{-3}$ over the Pacific west of North America for Dalsoren and Dentener emission. For the case of the southern part the case applies the same that, Atlantic west of South Africa has higher change in CDNC than the Pacific west of South America. Neither E5/M1-MADE no CAM3.0 has found the significant change in CDNC and cloud droplet effective radius for Dentener emission over the Pacific west of South America.

(iii) For approximately the same range of Oceanic altitude (0.6-1.1km for E5/M1-MADE) and (0.69-1.3km for CAM3.0) and the same emission inventory (Dentener et al., 2006) and the back ground field (no ship emission), the E5/M1-MADE values of CDNC are quite higher than that of CAM3.0. This can be better observed by looking the contribution due to shipping (table 2b), example in Atlantic west of North Africa; CAM3.0 has the contribution of only 3 cm^{-3}, while E5/M1-MADE has a great contribution of up to $11cm^{-3}$. Over the Atlantic west of South Africa the CAM3.0 has a contribution of less than $1cm^{-3}$ but the E5/M1-MADE has a contribution of 3 cm^{-3}, and the same case applies to North East Asia.

On considering the percentage changes in CDNC for the cited areas and levels (table 3a) we see that the CAM 3.0 has lower percentage changes as compared to E5/M1-MADE except at Pacific west of North America where the CAM3.0 has 1.05% as compared to 0.53% of E5/M1-MADE**.** Based on these examples which are cited on areas with frequent shipping

traffic and characterized by the lower boundary marine liquid water clouds on average we can conclude that over Ocean E5/M1-MADE is more sensitive to change in CDNC than CAM3.0.

In case of changes in CDNC and R_e over the entire land masked Pacific and Atlantic Oceans for all levels assigned, the model results (tables 3b and 3c) reflect that still there is a high change in CDNC over the Atlantic Ocean than over the Pacific Ocean, also for all levels assigned E5/M1-MADE have higher changes in CDNC than CAM3.0. This is evidenced by models results (table 4c), that over the Pacific Ocean at altitude of (0.33-0.69 km) for CAM3.0 and (0.3-0.6 km) for E5/M1-MADE, where ΔN of 13.7 cm^{-3} for E5/M1-MADE is much higher than ΔN of 1.95 cm^{-3} for CAM3.0. Whereas for higher level ΔN of 4.2 cm^{-3} for E5/M1-MADE is three times higher than ΔN of 1.4cm^{-3} for CAM3.0. The case applies the same for the Atlantic Ocean where E5/M1-MADE have ΔN of 15.5 cm^{-3} for lower level and ΔN of 5.1 cm^{-3} for the higher level than ΔN of 2.5 cm^{-3} and 1.7 cm^{-3} for the CAM3.0. In view of the global mean, E5/M1-MADE results to ΔN of 5.9 cm^{-3} and 1.8 cm^{-3} which are higher than ΔN of 0.879 $cm^{-3}$and 0.167 cm^{-3} obtained by CAM3.0.

Based on these results of tables (2 to 3) we can conclude that over the ocean both models are more sensitive to changes in cloud droplet concentration over lower levels than over higher levels, but E5/M1-MADE is six to seven times sensitive at lower levels, and three times sensitive at higher levels than CAM3.0. The sensitivity of CAM 3.0 is decreasing oceanward and increases coastward, while E5/M1-MADE its sensitivity increases oceanward and decreases coastward.

These two model results from tables (2 to 3) bridges in the conclusion that E5/M1-MADE is more emission change sensitive (change in CDNC) over the Ocean than CAM3.0, and because the shipping effect concerned is stronger over the Oceans, it should be noted that the change in LWP (section 4.6.1) which has significant contribution to the change in net cloud forcing (section 4.8.1) depends on the change in cloud droplet number concentration (Storelvmo et al., 2006). Since we have seen that in the aspect of change of CDNC over the ocean E5/M1-MADE is six to seven times sensitive at lower level and three times sensitive at higher level as compare to CAM3.0, this argument could satisfy to be among the reasons as to why E5/M1-MADE net cloud forcing is three times higher than that of CAM3.0. Detailed summery of the suggested reasons explaining why E5/M1-MADE is more sensitive to the change in CDNC than CAM3.0 is presented in section 4.10

The emission totals of Wang et al., 2007 and Dalsoren et al., 2009, which are (9.28 Tgy^{-1} and 9.4 Tgy^{-1}) i.e. are approximately equal, but due to difference in model chemistry, vertical transport and aerosol schemes the two inventories have different results on changes of CDNC, R_e , LWP and hence SWCF (E5/M1-MADE values being higher than that of CAM3.0).

Through this example we can also conclude that irrespective of the emission inventory used, E5/M1-MADE is more sensitive to emission change than CAM3.0.

4.4.2 Zonal distribution of column CDNC

Model calculated results of zonal average column CDNC for annual and seasonal bases are represented by figures 8 (a) and 8 (b). Both figures, apart from supports the fact that NH is more affected by consequences caused by the shipping emission than the SH, but also represents the summer and winter shipping difference in NH (blue and black curves) as being supported by various recent studies including Skjolsvik et al., 2000; Endresen et al., 2003 a.o., see section 4.2.1.

Interestingly both figures have shown high column CDNC values over 30^0N - 60^0N which are known as strong storm track regions (Gettelman et al., 2008). These areas are characterized by deep layer clouds and deep localized convective clouds especially over summer periods.
Latitudes 20S - 0 -20N (tropical oceans) are characterized by low shipping contribution of column CDNC than NH mid to high latitudes. Over the SH low latitudes 0S -20S the seasonal variation of JJA and SON has increased up to 0.5 (+05) cm^{-2} where as the annual zonal mean column CDNC has risen up to 0.3E(+05) cm^{-2}. This increase of column CDNC reflects the increase in sulphate particles due to increased shipping traffic. Different from NH high latitudes, the SH high latitudes including the Antarctica are among clean areas in the changes of CDNC (Wall, 2005; Shirsat and Graf, 2009).

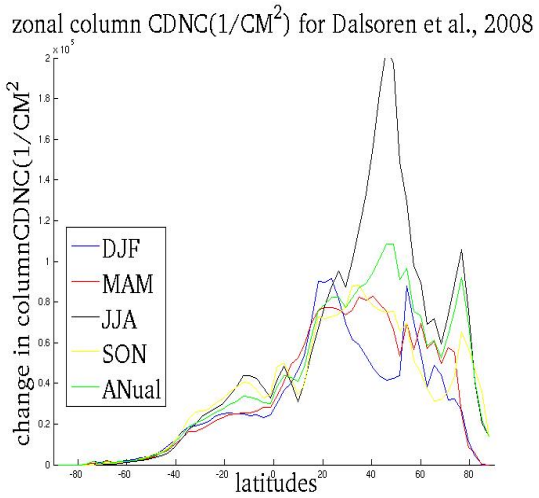

Figure 8(a)

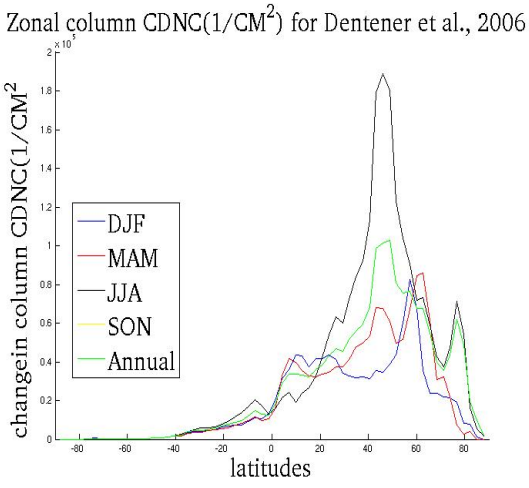

Figure 8(b)

Figure 8 (a & b) shipping contribution on zonal mean column CDNC for Dalsoren and Dentener emission.

4.5.1 Cloud droplet effective radius (R_e)

The R_e is one among the key parameters in determining the TOA SWCF and the net cloud forcing (Storelvmo et al., 2006). The decrease in R_e reflects the first indirect effect due to increased cloud reflectivity (albedo) caused by increased particle concentration injected into the cloud for a given volume of air and hence CDNC (see equations 1 and 3).

The annual global average R_e calculated by the model is 14.38 μm, 14.35 μm and 14.42 μm for Dalsoren, Dentener and no ship emissions. These model calculated values approximately compares well with 14 μm of Sekiguchi et al., 2003; Gettlman et al., 2008, but are slightly higher than 13.3 μm obtained by Storelvmo et al., 2006 using the CAM-Oslo and 10.31 μm calculated by Kristjansson et al., 2002 using the National Centre for Atmospheric Research Community Climate Model Version 3 (NCAR CCM3). The annual global average ship induced R_e is -0.0738μm equivalent to a decrease of -0.51% and -0.0395μm equivalent to decreases of -0.27% based on the inventory. This decrease in R_e is about 7% to 13% of the global mean reduction in R_e (of 0.58μm) of the total anthropogenic sulphate emission Kristjansson et al., 2002 and is well agreed by him that, the anthropogenic sulphate aerosols lead to a general decrease in cloud droplet size, resulting in large surface area of the droplet and hence enhances the CA.

This smaller reduction in R_e is due to slight changes of high model values LWP caused by newly inject aerosols which are smaller compared to aged particles existing in the cloud (Lauer et al., 2007). Comparison of this result with other studies which deals on effects of ship emissions on clouds has been difficult because most of these studies including Lauer et al., 2007; Taylor et al., 1997 and Coakley and Walsh (2001) do not provide the global contribution of neither CDNC nor R_e instead they were interested in localized area and specific levels.

The geographical variation of R_e has show high reduction in areas characterized by low liquid water marine clouds. The annual and seasonal (figures are not included) average geographical distribution of R_e due to shipping is more effective in coastal and Ocean areas characterized by dense ship traffic and low marine liquid water clouds. Example figure 9(a) has number of maximum peaks of up to -0.6 μm over Northern Atlantic at the areas of Gulf of Mexico, North Sea and the entrance of Baltic Sea, Norwegian Sea, Barents Sea and Svalbard at the Arctic Ocean.

Over Northern Pacific the peak is at West coast of North America west of Santa Cruz near the Gulf of Tehuantepec, where as in Indian Ocean the peak of up to -0.7 μm is obtained at the Gulf of Aden. Over the SH the only sub peak is obtained at the Atlantic South at the west coast of southern Africa. The peaks and sub peaks of up to -0.4 μm are mostly distributed over areas characterized by low marine liquid water clouds as stated by Lauer et al., 2007.

The percentage changes of R_e has high values ranging from -4 to –5.5% at Northern Atlantic, where as areas of Pacific Ocean, Southern Atlantic Ocean and Indian Ocean are subjected to lower percentage changes of 2-3%.

Referring to figure 1(a) you will notice that the area between Arctic Ocean and Greenland (both eastern and western) has low emission level, but figure 9a show that these areas has been induced with high reduction in effective radius of up to -0.6μm and percentage change of up to -3% (figure 9c) indicating that the perturbation of ($\Delta R_e/R_e$) have shown the susceptibility of the area due to emission change.

In figure 9b ship induced R_e is characterized by strong changes but with little coverage, the annual average change cloud droplet effective radius has highest peak of -0.9 μm over North Sea followed by -0.7 μm to -0.8 μm at the Gulf Aden, Arabian Sea and Red Sea.
More reflections to figure 9a and 9b reveals that there is an increasing trend of reduction in R_e over Southern due to increased ship traffic, where areas including west coast of Namibia, and some parts of Southern Mediterranean Sea have experienced a change of -0.2 to -0.3 μm.

Unlike figure 9c the percentage changes of R_e for figure 9d is mostly confined over Northern Atlantic with strong percentage increase of up to -7%, where as Southern and southeastern Asia are subjected to high reduction of -6 to -7%, where as western coast of Namibia is having a percentage change of only -2%.

The common feature shown by figures 9a-9d is the fact that, unlike the Arctic, the Antarctica is not highly affected by ship emission either direct or downwind from the nearby sources like south West Africa. Among other studies which support this argument is that of Shirsat and Graf, 2009, which deals inventory of sulphur emission based on Antarctica. Their results show that though there is an indication of human presence in this area but the amount of SO_2 emission due to shipping are very small as compared to other regions. Thus why the reduction in R_e has been small (compared to Arctic region) but significant over the region because figure 10a over the SH has the highest peak of ship induced R_e at this region (60S-80S).

Due to the fact that cloud parameters relate to each other (equations 1- 6) also their effect due to change in emission will resemble to each other. If we make comparisons with figure 7a and figure 9a you will find that these figure have the same pattern in almost most areas of high decrease in R_e are associated with the high increase in CDNC. Also these two figures support the finding by Kristjansson et al., 200 that the sulphate anthropogenic changes in ($\Delta R_e /R_e$) and ($\Delta N/N$) relates with each other.

The mode calculated global mean decrease in R_e for (JJA) season has raised up to -0.092 μm and -0.052μm, where as the geographical distribution (figures not included) has gone up -1

μm for some latitudes in both Northern Atlantic and Northern Pacific Oceans. For the North Atlantic Ocean at the belt from Gulf of Mexico to Europe including areas of North Sea, Baltic Sea and English Channel has experienced a change of up to -1 μm, where as areas including Portugal, Bay of Biscay est. has experience a change of -0.7 μm to -0.9 μm. Indian Ocean at the Arabian Sea has been subjected to a decrease ranging between -0.4 μm to -0.9 μm. Percentage change of -3% to -8% has been experienced on both Northern Atlantic and Pacific Oceans, where as Indian Ocean and Southern Atlantic (west coast of Namibia) has fall up to a change of -1% to -3%.

Figure 9(a)

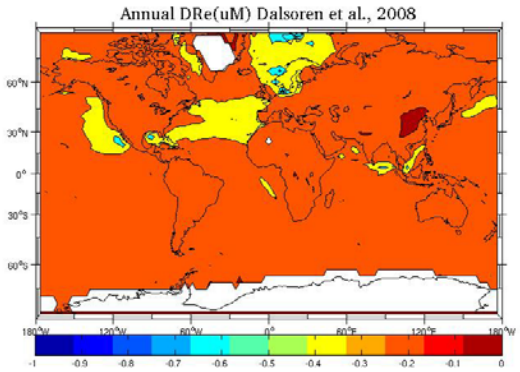

Figure 9(b)

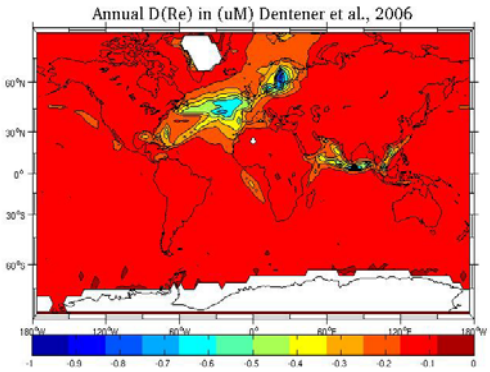

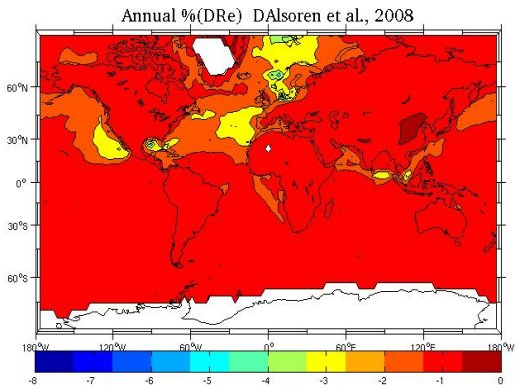

Figure 9(c)

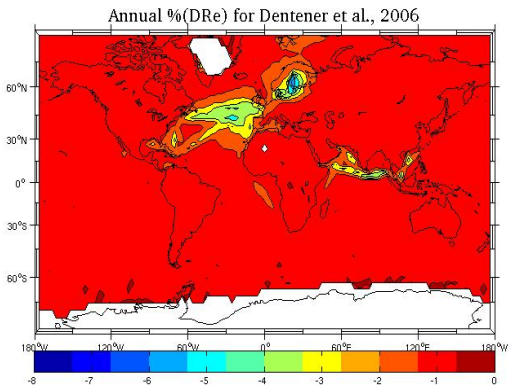

Figure 9(d)

Figures 9(a-d) are the ship induced relative and percentage changes in cloud droplet effective radius, Figures 9(a & c) annual relative and percentage changes due to Dalsoren et al., 2008; figures 9(b & d)) annual relative and percentage changes due to Dentener et al., 2006.

For the ship induced changes in size distribution and particle number concentration over lower troposphere, model simulation results for the changes in R_e and CDNC which are tabulated in tables (2 to 3) yields the following reflections/deductions.

(i) The CAM 3.0 has high values of R_e which are associated with high values of LWP for all inventories and levels than E5/M1-MADE. Example using Dentener emission the R_e ranges from 12.72 μm over North East Asia to 15.18 μm over South America, but for the same areas E5/M1-MADE has smaller values ranging from 8.58 μm to 11.70 μm. The case applies the same for all other cited areas and levels (refer table 2(a)), as agreed by Storelvmo et al., 2006 that the CAM –Oslo yields large cloud droplets with effective radii ranging from 14-16 μm over subtropical oceans and Arctic areas.

(ii) For the model levels 23:24, in contrast to the changes in CDNC the changes in R_e are higher in CAM3.0 than in E5/M1-MADE. Using table 2a the changes in R_e over Atlantic (for both North West and South west) Africa and over North East Asia are higher in CAM3.0 than in E5/M1-MADE. Also the percentages changes in R_e (table 3(b)) are higher in CA3.0 than in E5/M1-MADE. The highest percentage change in R_e has occurred over Atlantic North West Africa where CAM3.0 has a change of 1.61% as compared to1.44% of E5/M1-MADE, the situation remains the same for all other cited examples except over Pacific north of West America the pattern is different, where E5/M1-MADE has high percentage change in R_e and CAM3.0 have high percentage change in CDNC.

(iii) Over the Pacific Ocean, CAM3.0 has higher relative and percentage changes of R_e for all levels selected (table 3b), whereas over the Atlantic Ocean CAM3.0 has higher changes over higher levels and lower changes over lower level. The global mean changes in radius are nearly the same for lower model levels but higher in CAM3.0 for higher model levels.
In general 4/5 (or 80%) of the cited areas and selected levels CAM3.0 have higher percentage and relative changes in R_e while 4/5 (or 80%) of these areas E5/M1-MADE has higher relative changes and 60% higher percentage changes in CDNC. The tabulated data provides higher intra-model differences in the changes of CDNC and lower in the changes of R_e.

There is a slight oceanward increasing trend of changes in R_e in CAM3.0 and significant oceanward increasing trend of changes in CDNC in E5/M1-MADE. The influence of these changes of ΔN and $\%\Delta N$, ΔR_e and $\%R_e$ as well as ΔLWP and $\%\Delta LWP$ to the net cloud forcing (AIE) in relation to equations 4 to 7 has been discussed in detail in section 4.10.

From these cited examples (table 3a) we can conclude that E5/M1-MADE has higher relative and percentage changes in ΔN and $\%\Delta N$ which increases oceanward and approximately the same changes in ΔR_e and $\%\Delta R_e$ as CAM3.0, but in contrary CAM3.0 has lower changes in ΔN and $\%\Delta N$ which decreases oceanward and slightly higher changes of ΔR_e and $\%\Delta R_e$ which increases oceanward**.** Refer section 4.10 for the detailed summery relating ΔR_e and $\%\Delta R_e$ and $\mathbf{\Delta N}$ and $\%\mathbf{\Delta N}$ and the argument as to why E5/M1-MADE has net cloud forcing which is about three times higher than that of CAM3.0.

4.5.2 Zonal distribution of cloud droplet effective radius

Figures 10(a - b) are the model results for the zonal average R_e. Variations in decrease of cloud top R_e due to shipping contribution are confined to the latitudes having frequent ship traffic. Reflections from these figures show that there is a great decrease of up to -0.3 μm in JJA confined at latitude 40N, this is contributed by the fact that (i) the ship traffic is dense at all periods except during the DJF (which reflects an increase in R_e over the 35N to 45N caused by the decrease in ship traffic) season or NH winter period (ii) the area is among the highly polluted zone (either by direct shipping pollution or downwind from other shipping routes) with enhanced high CA influenced by high concentrations of SO_2 emission which is oxidized to sulphate particles refer figures 1a-1b and 3a-3d.

The general decrease of about -0.25 μm for all seasons including annual (except for the DJF) variation is confined at latitude 60N to 80N, followed by a rapid raise at latitude 80N. Interestingly there is a significant increase in R_e roughly at latitude 45N to 65N (indicating the decrease in pollution). Unlike figure 10a figure 10b reflects the sharp decrease of up to -0.45 μm followed by an increase at the latitudes between 80N to 90N. This supports our argument that unlike SH Antarctic the NH Arctic is not safe from the effects of ship emission. Over the SH figure 10a reports a general decrease in radius of up -0.05 μm at 10S to 30S for all seasons including the annual. But in contrast with figure10(b) which show a decrease in radius (of up to -0.1 μm) for the latitude zone of 10N-0S -10S, for the periods of JJA, MAM, DFJ and the annual, figure10(a) reports a slight increase in radius (of up to -0.025 μm). Both inventories have seasonal variation in R_e with its peak value at JJA over the NH where as the figure 10a show an increase trend of the effect due to increased shipping traffic over the SH.

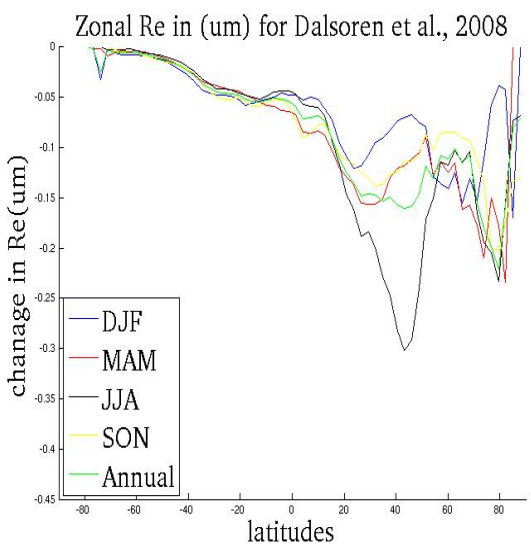

Figure 10(a)

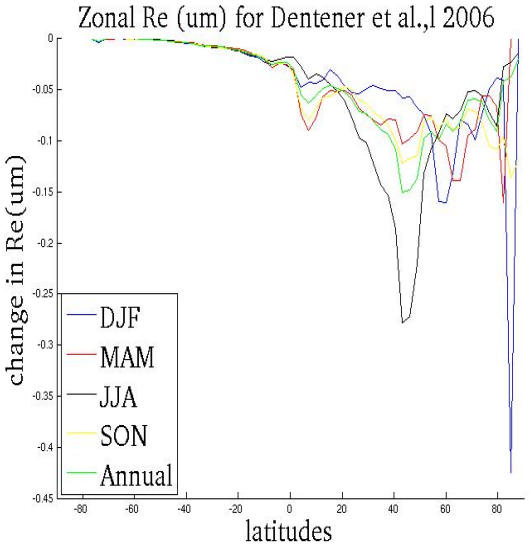

Figure 10(b)

Figure 10(a &b) the ship induced changes in zonal cloud top effective radius

4.6.1 Integrated cloud Liquid water Path (LWP)

The LWP in (gm^{-2}) which is among the crucial parameters in calculating both the radiative forcing of the clouds (Storelvmo et al., 2006) was simulated by the model. This parameter largely depends on activation (for a given super saturation level) which determine the amount and size of CDNC (refer equations 2, 3 and 4). The result of ship induced LWP which largely varies with geographical and hemispherical orientations (latitudinal variations) are presented in annual, seasonal, zonal and regional basis.

The annual global mean LWP is 128.88 gm^{-2} and 129.01 gm^{-2}, where the contribution due shipping is 0.18 gm^{-2} equivalent to 0.14% and 0.31 gm^{-2} equivalent to 0.24%, and for the back ground cloud the (no shipping emission) the global average LWP is 128.70 gm^{-2}. These model values of ship induced %LWP contribute to 3% and 5% of the global mean percentage contribution due to anthropogenic sulphate emission calculated by Kristjansson et al., 2002.

This model back ground value compares well with (124.7 and 130.5) gm^{-2} measured out of the ship track in Monterey Area Ship Track (MAST) campaign (Taylor et al., 1997) using microwave radiometer and near-infrared reflectance. While the values of (188.8 and 177.6 gm^{-2}) measured in (or inside) the ship track by the same instruments are larger than our model calculated global mean values of (128.88 and 129.01 gm^{-2}), but this can't be a fair comparison because the shipping signal can't be easily evaluated by single-point measurements (Lauer et al 2007; Eyring et al., 2007). But when compared to somB and somBco_2 (Kirkevaag et al., 2007) our total atmospheric model values for the LWP are higher than (113.7 and 115.3 gm^{-2}) of somB and somBco_2 respectively.

When we compare the %LWP obtained from CAM3.0 with that obtained from E5/M1-MADE over Pacific and Atlantic Ocean we find that CAM3.0 values of (0.41% - 0.49% table 3(c)) are very low compared to (1-2%) of E5/M1-MADE. This high intra model difference in ship induced %LWP is due to the fact that CAM3.0 has smaller changes in ΔN and %ΔN (over Ocean) which results in smaller changes in ΔLWP and %ΔLWP, but E5/M1-MADE allows the higher % ΔLWP because: (i) it has a large percentage increase of 15% (Lauer et al., 2007) for the accumulation mode particle number concentration at the lowest boundary layer compared to 3% and 5% obtained by CAM3.0 (ii) from equation (2) for a giver super saturation level and fixed LWC the high % increase in particle number concentration enhances a high increase in CDNC associated with decrease in R_e and increase in LWP and vice- versa) large changes in ΔN and %ΔN (over Ocean) resulting in relatively higher changes in ΔLWP and %ΔLWP refer tables (2, 3 & 4) .

The seasonal global mean LWP is higher for JJA. If we refer to previous sections we will find that the sulphate burden, CDNC, (AOD, COD and CA), R_e and LWP, all have both global and zonal mean values higher in JJA. The reason behind is due to the fact that during this period the rate of ozone production at NH mid to high latitudes is high due to increased ship traffic (Dalsoren et al., 2008). Ozone which has the roles of (i) production of hydroxyl (OH) radical which in turn oxidizes the SO_2 in the gaseous phase to produce sulphate particle (ii) to combine with hydrogen peroxide (H_2O_2) in the aqueous phase of cloud droplets, and produces sulphate particle (Lauer et al., 2007; Dalsoren et al., 2008). Apart from (i) and (ii) using equation (5 and 6) we calculated the contribution of COD and CA at the annual and seasonal JJA and find that global mean value of COD exceeds that of annual by 5% and 6%, and its contribution to the annual is 30% and 31%, where as for CA the ship induced value contribute by about 28% and 31% of the annual global mean CA (refer section 4.3.1)

In quantifying this arguments ((i) and (ii) above) of having more sulphate particles (CCN) in JJA season due to increased ozone, the model calculated results of annual and seasonal (JJA) percentage increase in sulphate nucleation rate (i.e. sulphur mixing ratio per second i.e. formation of new particles per second) at model levels 23:25 show an annual percentage increase of 5% and 7%, and seasonal percentage increase of 6.9% and 7.0% equivalent to 36% and 25% of the annual global % increase based upon the inventory used. Furthermore the geographical distribution of the sulphate nucleation rate at an altitude of (0.33-1.3)km, reveals that the sulphate nucleation rate is mapped over the Ocean (figures not included) with the highest values and coverage obtained in JJA.

The global mean ship induced LWP for JJA period is $0.4gm^{-2}$ and $0.24gm^{-2}$. These model values contribute to 33% and 32% of global mean ship induced LWP. In reference to section 4.5.1 we have seen that the annual % change in R_e ranges from 0.27% to 0.51%, while in this

section we have seen the annual % change in LWP ranges from 0.14% to 0.24%, since these two crucial parameters for determining the changes in both SWCF and the LWCF (Storelvmo et al., 2006) are low, our expectation for the net cloud forcing is also low.

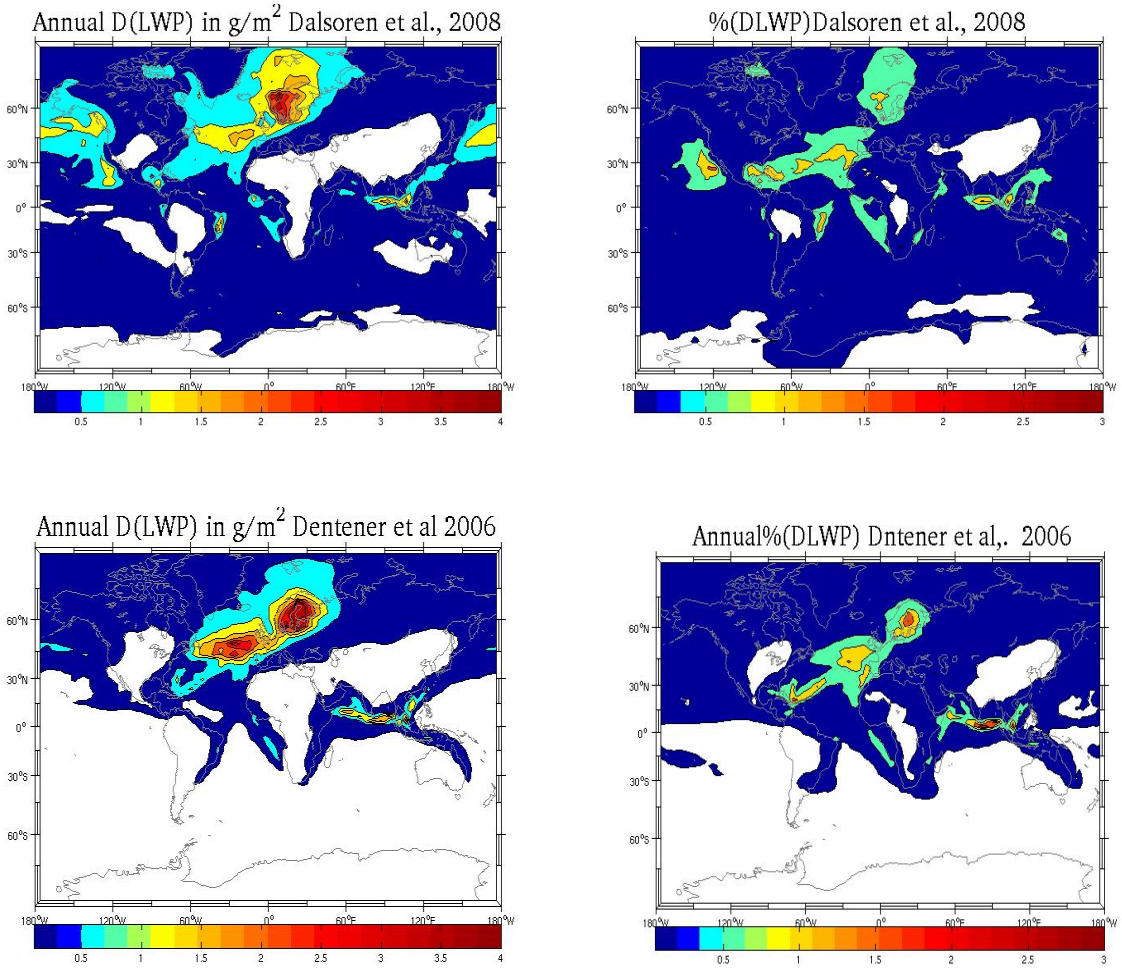

Figures 11(a-d) are the relative and percentage changes (ΔLWP and %ΔLWP) due to shipping, first row figures 11(a & b) annual relative and percentage changes in liquid water path for Dalsoren et al., 2008; second row figures 11(c & d) annual relative and percentage changes for Dentener et al., 2006. Note that for figures representing relative changes the dark blue in color bar is defined by $0.1 \leq x < 0.5 gm^{-2}$ and the white area is less than 0.1. For the % changes dark blue is defined by $0.05 \leq x < 0.5\%$ and the white areas are less than 0.05%

In dealing with more frequent ship traffic areas with high amount of low clouds above the Oceans (i.e. susceptible areas) model simulates the change in ΔN (cm^{-3}), ΔR_e (μm) refer table (3c) and ΔLWP (gm^{-2}) over the Pacific and Atlantic Oceans for the model levels 23:24 and 24:25. Table (4) show that LWP which has increased up to 0.41% and 0.49% over the Atlantic Ocean and up to 0.34% and 0.41% over the Pacific Ocean based on the inventory used. The results of R_e in table (3c) and that of LWP in table (4) reflects the influence of

these areas to be susceptible to changes in emission, hence caused high net cloud forcing over both Atlantic and Pacific Ocean (see section 4.7.1).

The annual geographical distribution of the ship induced LWP, for both inventories have maximum peak at Baltic Sea of up to 3.5 gm^{-2} figure (11(a & c)), but figure 11(a) has many distributed sub maxima of 1.5- 2 gm^{-2} over different shipping areas, where as figure11(b) has sub maxima which mostly confined over Northern Atlantic. The seasonal ship induced geographical distribution for this parameter over JJA has peaks of up to 5gm^{-2} over the Northern Pacific (figures are not included), and distributed sub maxima over the western coast on North America at Pacific ocean, and the Northeastern part of Asia.

The annual %ΔLWP increase due to shipping has many distributed peaks of 1 to 1.5%. The interesting feature shown by figure 11(b) is that most of the areas having the peak % change of the LWP coincides with areas dominated by the low marine liquid water clouds over frequent ship traffic areas (refer Lauer et al., 2007 page 5072 figure 9). In general CAM3.0 simulation results has shown the low values for annual % increase in ship induced LWP and % geographical distribution both global and specified regions (Pacific and Atlantic Ocean).
Regarding the relation of LWP and CDNC (equations 2, 3 and 4), this can be clearly explained by the fact that CAM3.0 has small % change in number concentration of the accumulation mode size sulphate particle which acts as efficient CCN, and which is a suitable size for the activation to higher droplet size depending on the super saturation level

4.6.2 Zonal distribution of liquid water path

For the zonal distribution the model simulated results for LWP show the latitudinal agreement with all other simulated parameters, that the high shipping effect is observed over NH mid to high latitudes (30N -60N) or the storm track regions (Eyring et al., 2009), with little effect in the SH. This distribution has the higher values over the same areas as that of CDNC. The highest value for the mean zonal annual distribution is 0.7gm^{-2} and 0.65gm^{-2}, where as JJA has highest value of up 1.1gm^{-2} and 0.9gm^{-2}. Over high ship traffic areas the zonal difference in LWP between the annual and the seasonal (JJA) is higher for both inventories. This indicates that effects of shipping on cloud is higher over JJA, and is more confined at the NH mid to higher latitudes.

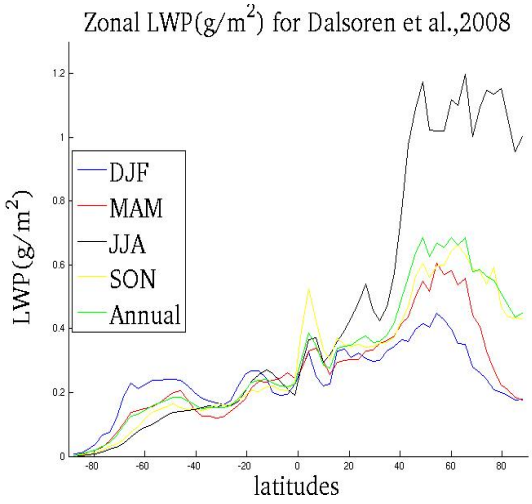

Figure 12(a)

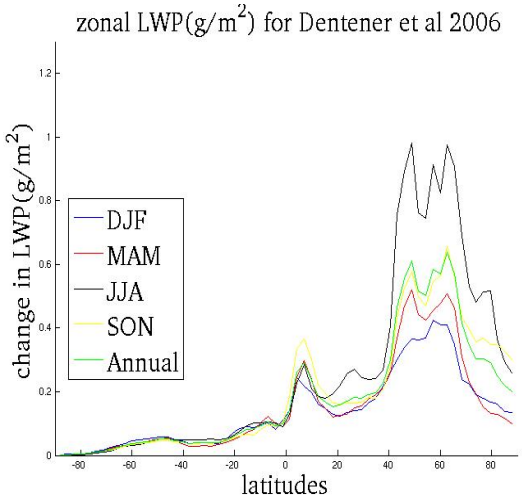

Figure 12(b)

Figures 12(a-b) are the ship induced zonal distribution of LWP for Dalsoren et al., 2008 and Dentener et al., 2006 shipping inventories.

The DJF (NH winter period) seasonal fluctuation has lowest values of column CDNC (figure 8(a & b)), causing the LWP (figure12 (a &b)) to be the lowest over this period, where as the R_e (figure 10(a & b)) reflects an increasing trend over the NH storm track regions due to reduced ship traffic over Winter period. In contrast to figure12b, figure 12a has reported the increase of LWP over the SH, with the DJF being leading with highest zonal mean value of about 0.25 gm^{-2} over higher latitudes between 40S to 60S.

4.7 Long wave cloud forcing (LWCF) in (Wm^{-2})

The LWCF or thermal spectral response is more affected by the change of LWP (Storelvmo et al., 2006) and contributes more to the second indirect effect. The model simulated results yields the values which are in good agreement with other studies. The global annual average long wave cloud forcing is 29.1939 Wm^{-2} and 29.1941 Wm^{-2} for Dentener and Dalsoren shipping inventories (present- day values), where as for the back ground model cloud or (pre-industrial value) the value is 29.1937 Wm^{-2}. These values are slightly higher than 28.0 Wm^{-2} obtained by E5/M1-MADE, but are slightly lower than 29.3 Wm^{-2} obtained by (ERBE) satellite retrievals. From these model results the shipping contribution on LWCF is about 0.0002 Wm^{-2} equivalents to 0.0007% and 0.0004 Wm^{-2} equivalents to 0.00140%. Due to this very small positive contribution on LWCF, the net cloud forcing at TOA has been generally taken to be equal or equivalent to the SWCF, as suggested by Storelvmo et al., 2006.

In principle the cloud-topped boundary layer without upper level clouds, has the long wave radiative cooling at the cloud top as a main source for the turbulence, where the energetic turbulent eddies effectively transport the cooled air near the cloud top down to the ground causing in a strong sensible heat flux at the surface. For multilayered clouds, radiative cooling

at the lower-level cloud top is significantly reduced due to the enhanced downward long wave radiative flux above the cloud, leading to a higher temperature of surface air and weaker positive sensible heat flux at the surface.

This situation is highly determined by the amount of cloud LWP. The emission of LWCF from clouds is exponentially related to cloud LWP, where as for large LWP the cloud acts as a blackbody leading to decrease both the spectral and long wave sensitivities (Dan et al., 2006). Before the threshold value of LWP cloud emissivity also increases with the decrease in effective radius (Dan et al., 2006). In case of SWCF the emissivity infinitely increases as the cloud LWP increases i.e. no threshold value which limits or saturates the cloud emissivity of SWCF.

This argument holds for small model calculated values of ship induced LWP and R_e (table(5)) which enhanced the cloud to emit low ship induced LWCF of the order of 10^{-4} Wm^{-2} indicating that radiative impacts of shipping emission affects more outgoing short wave radiation than the long wave radiation. This is because (i) the water clouds have cloud top temperature which does not differ much from that of the underlying surface temperature Kristjansson et al., 2002; Lauer et al., 2007 (ii) The respond of LWCF to LWP is exponential related. Though the ship induced LWCF is very small but its zonal mean characteristics (figures are not included due to lower contribution on AIE) reflects the same fact that tropical to subtropical Oceans (20S – 0 - 20N) are characterized by relatively high ship induced changes in LWCF, also the NH mid to high latitudes (60N to 80N) are having high effects of shipping than SH. This distribution of ship induced LWCF have shown great reduction over the latitude zone of 20N to 40N.

4.8.1 Short wave cloud forcing (W/m^2)

The SWCF contributes to around 99.7% of the AIE. The AIE largely depends on the changes of ΔR_e (which enhances the change in COD and CA equation 5 and 6) and slightly the change in ΔLWP (equations 2 and 4), Other factors which determine the large geographical variation of AIE are the cloud distribution, cloud height, aerosol distribution, surface albedo and solar zenith angle (Kristjansson et al., 2002).

The model simulated results of SWCF in annual, hemispherical, seasonal, and zonal as well as regional have been analyzed and plotted in both geographical and zonal orientations. The annual global mean SWCF is -53.75 Wm^{-2}; -53.81 Wm^{-2} and -53.69 Wm^{-2} for Dentener; Dalsoren inventories, and no shipping emission. These model results are in good agreement with other studies including those which used CAM-Oslo as their tool of analysis among others are: -54.7Wm^{-2} in CAM3.0 of Collins et al., 2006a; -55.1 Wm^{-2} of Seland et al., 2007; -54.1Wm^{-2} of Harrison et al., 1990; Kiehl and Trenberth, 1997 whom they used the Satellite data from Earth Radiation Budget Experiment (ERBE)) and -52.9 Wm^{-2} of Lauer et al., 2007

using the E5/M1-MADE model. Here you will find that our values for global annual short wave cloud forcing at (TOA) even though comparable but are slightly higher than that of Lauer et al., 2007.

The global mean ship induced SWCF at TOA is -0.063 Wm^{-2} equivalent to 0.12% and -0.121 W/m^2 equivalent to 0.23% (see table 5). This AIE of -0.063 Wm^{-2} for CAM3.0 is smaller by a factor of three than -0.19Wm^{-2} calculated E5/M1-MADE using the Dentener shipping inventory, and smaller by a factor of two to that obtained by the same model CAM3.0 using the Dalsoren shipping inventory. This model value of AIE due to shipping contributes to 15% and 30% of the mean shipping radiative components (-0.409 Wm^{-2}) for the year 2005 given by Eyring et al., 2009, also contributes to 9% and 17% of the global mean total indirect radiative forcing of (-0.7 Wm^{-2}) for the year 2005 (IPCC, 2007). Furthermore this model calculated indirect effect due to shipping contributes to 4% and 7% of the global mean anthropogenic sulphate AIE (of -1.8 i.e. life time and radius effect) calculated by Kristjansson et al., 2002.

The changes in the cloud microphysics had significant impacts on the cloud radiative forcing, in reference to equations (2, 3, 4 and 5), and the model results of microphysical parameters can briefly explains why our value for the SWCF is small i.e. it is due to smaller contribution of model calculated relative and % changes of these parameters including R_e of (-0.0395μm or -0.27% and -0.0738 μm or -0.51%) and LWP of (0.18 gm^{-2} or 0.14% and 0.31 gm^{-2} or 0.24%) based on the inventory. In concerning with the above mention equations the decrease in R_e enhances the increases of CA (equation 5 and 6) due to increased cloud droplet surface area which causes more reflection of the short wave solar radiation. This impact is in agreement with the Monterey Area Ship Track 1994 (MAST) where, when their cloud droplet size was reduced (in clean areas) the drizzle was suppressed due to increased competition for the LWP in the polluted ship track environment, and the net effect of changes in R_e and LWP was to increase the CRF by a factor of 4 Taylor et al., 1997.

For the dense traffic areas including the land masked Pacific and Atlantic Oceans, the model calculated ship induced net cloud forcing over the Pacific Ocean is -0.185 Wm^{-2} and -0.143 Wm^{-2} equivalent to 1.5 and 2.3 times the global mean shipping contribution, whereas over for Atlantic Ocean the shipping contribute to -0.242 Wm^{-2} and -0.188 Wm^{-2} equivalent to about 2 and 3 times the global mean values of the used inventoried (see table (4)).

For the LWP over the Pacific Ocean(refer section 4.6.1) the contribution due to shipping has been increased by a factor of 1.32 and 1.9 times the global mean value, whereas over the Atlantic Ocean the shipping contribution has been increased by a factor of 1.58 and 2.3 times the global mean value of the used inventory. Further reflections on these model results show that effects of shipping on clouds over dense traffic Oceans is higher than global mean effects.

Note that our regional results for the Atlantic and Pacific Oceans are also lower by a factor of 3 than that of E5/M1-MADE.

Table (4) annual mean ship induced changes of SWCF (Wm^{-2}) at TOA, numbers in parenthesis are E5/M1-MADE results Lauer et al., 2007. Grid boxes are defined in tables (3(b) and 3(c)).

Emission	Pacific Ocean		Atlantic ocean		Global mean	
	NetWm^{-2}	%ΔLWP	NetW/m^2	%ΔLWP	Net(Wm^{-2})	%ΔLWP
Dentener	-0.143 (-0.46)	0.34 (1-2)	-0.188 (-0.60)	0.41 (1-2)	-0.063(-0.19)	0.14
Dalsoren	-0.185	0.41	-0.242	0.49	-0.121	0.24

For JJA seasonal variation, the model simulated results on SWCF reflect on the impact of higher emission totals, which triggers higher column CDNC (section 4.4.1) associated with great reduction of R_e (33 - 31% refer section 4.5.1) i.e. increasing the CA (33%-35% refer section 4.3.1) and hence induced higher changes in column LWP (33% to 32% refer section 4.6.1) and cause the combined net effect of increasing AIE over the season.

Due to various factors in which AIE depends on (as mentioned above) and based on the reasons listed in section (4.6.1) including the high percentage contribution on the amount of radiation for JJA. The ship induced SWCF for JJA has risen from annual global mean of (-0.063 Wm^{-2} and -0.121 Wm^{-2}) up to seasonal global mean of (-0.102 Wm^{-2} and -0.187 Wm^{-2}) showing an increase of (-0.039 Wm^{-2} or 15% and -0.066 Wm^{-2} or 14% of the global mean SWCF), i.e. this season SWCF due to shipping is (1.62 and 1.55) times the annual global value of the used inventories (see table (5)). In comparing with other seasons (DJF, MAM, JJA and SON) this season has the highest contribution of about 40% and 39% of the global mean SWCF. This high radiative and microphysical effect not only reflects the reasons mentioned in section 4.6.1, but also the maximum solar insolation time especially over the NH which is characterized by more land cover.

On examining the influence of increased sulphur emission level over the SH (section 4.1.1), the model simulated results for SWCF over this region is more sensitive to Dalsoren shipping inventory than the Dentener. The annual hemispherical average shipping contribution for SWCF over the SH is -0.021 Wm^{-2} and -0.065 Wm^{-2} depending on the inventory, These values are about 17% and 27% of the global average annual ship induced net cloud forcing (see table 5). This % contribution of SWCF due to Dalsoren over SH is about 1.7 times that of Dentener, showing an increase of the radiative effect of clouds which can be explained by the fact that, though SH is not highly polluted but its background cloud microphysical conditions are susceptible to emission changes, causing the level of impact to be raised as supported by Taylor et al., 1997.

Tables (5 and 6) give a clear picture on how (i.e. to what extent) the shipping emissions affect the microphysical and radiative properties of clouds, and reflect on both the first and second indirect effects of the emissions (aerosol) on clouds. In global context the lowest contribution of the net cloud forcing (due to shipping) occurs in the SH summer period (DJF). Over NH this period is characterized by long periods of low temperature associated with ice and snow falls hence limiting the frequency of ship traffic.

Table (5) the model results for cloud parameters including SWCF (wm^{-2}), $R_e(\mu m)$, LWP and column CDNC and their percentage % contribution relative to the annual mean shipping contribution . Bolded numbers in parenthesis are the % contribution to the annual SWCF.

	The global mean value and their percentage shipping contributions						
Variable	Net(wm^{-2})	$\Delta R_e(\mu m)$	$\%\Delta R_e$	$\Delta lwp(gm^{-2})$	$\%\Delta lwp$	$\Delta N(Ncm^{-2})$	$\% \Delta N$
Dentener	-0.063	-0.0395	-0.271	0.18	0.14	0.0258e(+6)	1.08
Dalsoren	-0.121	-0.0738	-0.509	0.31	0.24	0.0446e(+6)	1.87
	The seasonal changes for (JJA) or the Northern Hemisphere summer period						
Dentener	-0.102(**40%**)	-0.0520	32.91	0.24	33	0.0372e(+6)	36
Dalsoren	-0.187(**39%**)	-0.0921	31.16	0.40	32	0.0587e(+6)	33
	The hemispherical changes on the southern hemisphere						
Dentener	-0.021(**17%**)	-0.0117	14.81	0.06	17	0.00683e(+6)	13
Dalsoren	-0.065(**27%**)	-0.0407	27.57	0.18	29	0.0228e(+06)	26

In contrast to NH, over the SH, DJF period is characterized by humid atmospheric conditions associated with localized deep convective clouds. For this season the peak ship induced net cloud forcing is observed at SH regions of (0 to 20S) and (60S to 80S) see figure 14(a), this is influenced by increased traffic of bulk ships at high southern latitudes (Dalsoren et al., 2008) i.e. this high contribution of cloud forcing is due to ship traffic to and from Antarctica

Table (6) the model results for the seasonal variation of cloud parameters including SWCF (wm^{-2}), $R_e(\mu m)$, column LWP (gm^{-2}) and the column CDNC ($N\ cm^{-2}$) and their % contribution relative to the annual contribution. Bolded numbers in parenthesis are the % contribution to the annual SWCF cloud forcing.

	The seasonal changes for December, January and February (DJF)						
Variable	Net(wm^{-2})	$\Delta R_e(\mu m)$	$\%\Delta R_e$	$\Delta lwp(gm^{-2})$	$\%\Delta lwp$	$\Delta N(Ncm^{-2})$	$\%\ \Delta N$
Dentener	-0.034(**13%**)	-0.0262	17	0.14	19	0.0185E(+6)	18
Dalsoren	-0.079(**16%**)	-0.0563	19	0.26	21	0.0351E(+6)	20
	The seasonal changes for March, April and May (MAM)						
Dentener	-0.060(**24%**)	-0.0381	24.36	0.15	21	0.0213E(+6)	21
Dalsoren	-0.113(**23%**)	-0.0727	24.76	0.28	23	0.0390E(+6)	22
	The seasonal changes for the September, October and November (SON)						
Dentener	-0.053(**21%**)	-0.0405	26	0.18	25	0.0258E(+6)	25
Dalsoren	-0.101(**21%**)	-0.0729	25	0.30	24	0.0443E(+6)	25

The geographical distribution on ship induced SWCF figure 13(a-b) show more effects of shipping are mapped over North Atlantic Ocean, but figure 13(a) show the highest peak value of about -1.5 Wm^{-2} to -2.5 Wm^{-2} over the west coast of North America at the Tehuantepec bay near Santa Cruz and in Northern Pacific Ocean and at Baltic Sea for the Northern Atlantic Ocean. Other sub peaks of up to -1 Wm^{-2} are mapped in both Oceans mostly over the northern parts including areas of Californian Gulf, Gulf of Mexico, the west coast of Portugal and Spain, the North Sea and Baltic Sea, where as in the Southern Atlantic the West coast of South Africa at Durban. Over the Indian Ocean Gulf of Aden and east coast of North East Asia are characterized by a change of up to -1 W/m^2. For figure 13(b) the highest changes of up -2 W/m^2 to -2.5 W/m^2 occurred at Baltic Sea followed by -1.5 W/m^2 at the west coast of Portugal and Spain.

The highest changes in ship induced SWCF (of up to -4.5 W/m^2) are obtained during the JJA seasonal period (figures are not included) and they are more confined over the NH (for both Atlantic and Pacific Oceans) with small changes mapped to the SH. Over this period not only areas with high emission rates but also some low emission rate and clean areas are affected by

high changes in SWCF, areas including the Californian Gulf and others are among the affected.

Figure 13(a)

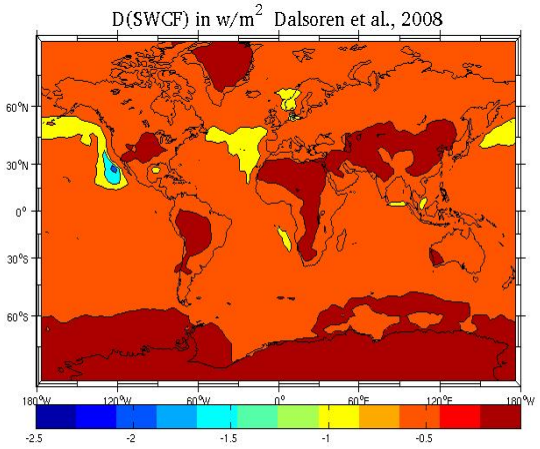

Figure 13(b)

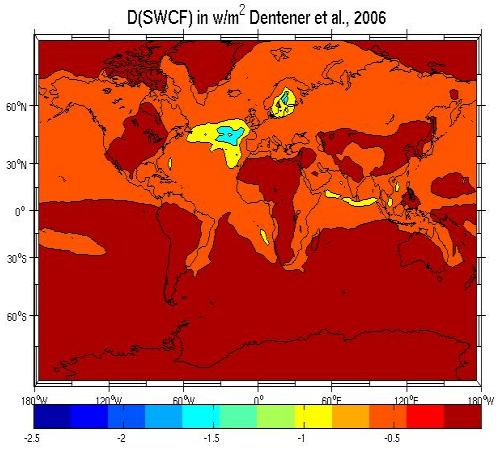

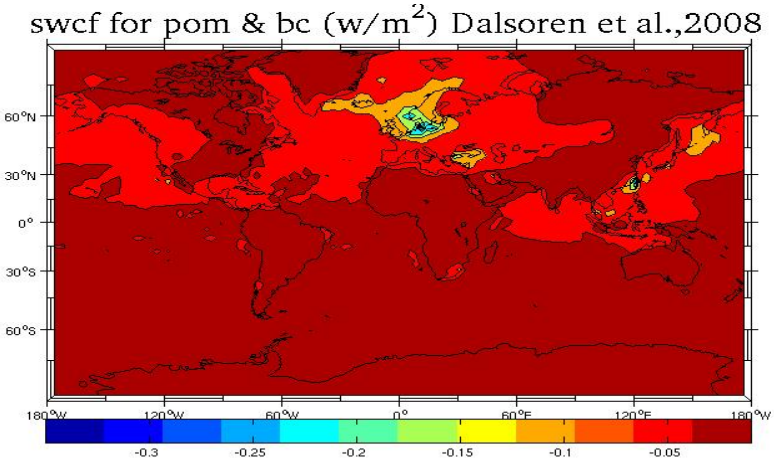

Figure 13(c)

Figures 13(a-b) are the ship induced changes on short wave cloud forcing. Figure 13(c) The contribution of POM and BC on short wave cloud forcing. Note in Figure 13(c) the dark red represents the values of $-0.01 \leq x < 0.05$ Wm^{-2}, where as in figure 13(a-b) the dark red represents the values $-0.02 \leq x < -0.05$ Wm^{-2}.

4.8.2 Zonal mean distribution of SWCF

In the context of the zonal variations, figure 14 (a & b) are the results of model calculated zonal averages on SWCF. This zonal mean distribution due to shipping has its peak value over the latitudes which are characterized by high ship traffic (Lauer et al., 2007) and storm

track regions (Gettelman et al., 2008) with more effect over the NH than SH. The annual and most seasonal zonal mean for MAM, JJA and SON have their peak value at latitudes ranging from 40N to 60N, but DJF has its peak values of up to -0.15 Wm^{-2} over the SH tropical region (0S to 20S) and high latitude region (60S to 80S) figure 14(a).

Both figures for all simulations (annual and seasonal) show high values of ship induced SWCF at the subtropical regions of 20S to 20N, as in agreement with the findings of Gettelman et al., 2008; Rasch and Kristjansson, 1998. More reflections show that figure 14(a) has influence an increased amount of SWCF over the SH than figure 14(b).

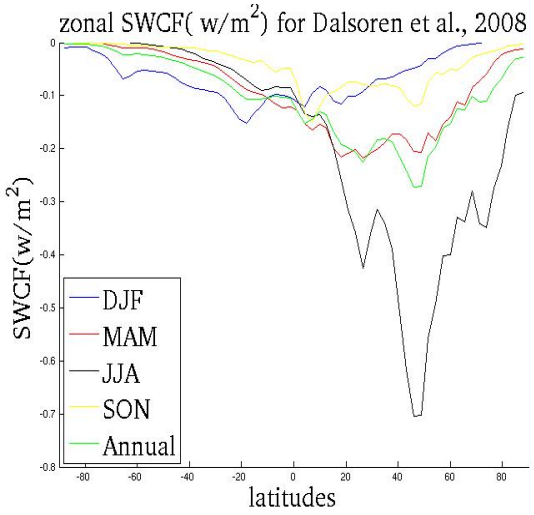

Figure 14(a)

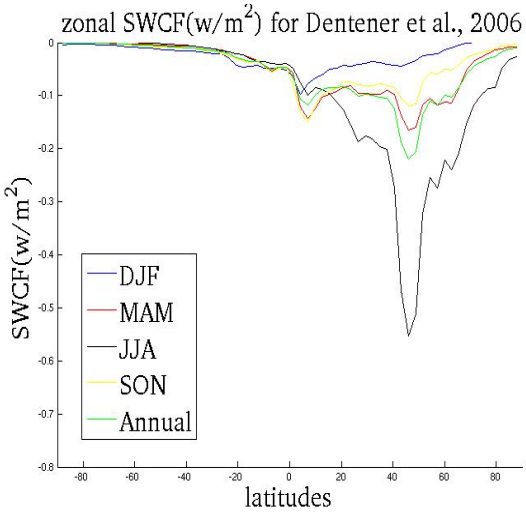

Figure 14(b)

Figures 14(a & b) the ship induced zonal distribution for the annual and seasonal average on SWCF due to Dalsoren and Dentener emission inventories.

The highest values of the zonal mean shipping contribution are seen over the JJA season (black curve), which have values ringing from -0.5 Wm^{-2} to -0.7 Wm^{-2} and are well agreed by both table (5) and figures 14(a& b) that, this seasonal period have high percentage contribution of SWCF ranging from 40% and 39% of the annual mean ship induced SWCF (green curve)

The zonal plots of cloud droplet effective radius (figure 10(a & b)), integrated cloud liquid water path (figure 13(a & b)) and SWCF figure 14(a & b), all have their high values at mid to high latitudes especially (40N-60N) showing high ship induced aerosol loadings as a result of dense ship traffic (over the region) or downwind advection from shipping routes in this latitude zone causing high changes in microphysical and radiative properties of cloud. This is well agreed by recent studies including Lauer et al., 2007; Storelvmo et al., 2006; Eyring et al., 2009 and more others.

4.9 Contribution of POM and BC

This sensitivity experiment of removing POM and BC in the background cloud model or no ship emission is mainly aimed to be among the reasons as why the CAM3.0 AIE is lower than that of E5/M1-MADE. In this experiment both of two (POM and BC) were removed at a goal and not one at a time. Note that the first offline simulations which we have conducted were including these ship emitted particles in all three emission inventories (i.e. Dalsoren, Dentener and the no shipping emissions).

Organic particles (POM and BC) has not only contributed to the increase on the amount of CCN by either externally or internally mixing with ship injected sulphate particles, but also they are responsible for influencing the CCN growth rates by enhancing the number concentration of particles containing sulphate and redistribute sulphate to lager and more active particle size (Shantz et al., 2008; Bilde and Svenningson, 2004; Lohmann et al., 2004).
In general organics play an important role in the cloud activation when internally mixed even with small amounts of sulphate and sea salt, as agreed by Abbatt et al., 2005; Bilde and Svenningson, 2004 Lohmann et al., 2004, that addition of even few percent of inorganic material (by mass) to a mostly insoluble organic can have a large impact on the CCN activation.

In reference to equation (11) if TOA SWCF of the pre-industrial and the present-day emissions are relatively high AIE will be small. In order to have large value of AIE we have to limit the increase in the amount of CDNC by either limiting the LWC i.e. limiting the activation scheme or remove the aerosol particles (aerosol pre-casers) which influence the growth rates of CCN into CDNC. Hence removal of the POM and BC in the back ground emission is among the simple and convenient alternative.

In estimating the role of organics in shaping the properties of clouds, the sensitivity experiment aimed at calculating the percentage shipping contribution of organics to AEI was conducted. The model simulated results for these organic particles from simulation with and without BC and POM are 0.1275 Tg and 0.1249 Tg for BC, where ship induced burden for BC is 0.0026 Tg equivalent to 2% of the total BC burden. This model calculated values compares well with E5/M1-MADE results of 0.122 Tg with ship contribution of 1.4% of the total BC burden. For POM the total burden is 1.1598 Tg and 1.1536 Tg, and the shipping contribution for POM is 0.0062 Tg equivalent to 0.5% of the total POM burden. Comparatively this model value is slightly higher than E5/M1-MADE results of 1.047 Tg with ship induced of 0.1%. These present- day model calculated values for the BC and POM are slightly lower, but at the same order of magnitude with that of 0.14 Tg and 1.31 Tg calculated by Seland et al., 2007 with CAM –Oslo.

Table (7) the changes of microphysical and radiative parameters due to ship emission with and without POM and BC in the no ship emission. Note the data in rows 4 and 7 are for the changes due to Dentener, where as that of rows 5 and 8 are the changes due to Dalsoren, data in row 2 are the changes due to no ship emission.

SWCF(wm^{-2})		LWCF(wm^{-2})		LWP(gm^{-2})		CDNC(cm^{-2})		R_e(μm)	
-53.686	-53.676	29.1937	29.1936	128.70	128.64	2.388E(+6)	2.384E(+6)	14.42	14.43
Shipping contribution on parameters with and without pom and bc for Dalsoren and Dentener emission									
-0.063	-0.073	-0.00002	-0.00003	0.18	0.24	0.02577E(+6)	0.02967E(+6)	-0.039	-0.046
-0.121	-0.131	-0.00004	-0.00005	0.31	0.37	0.04456E(+6)	0.04846E(+6)	-0.073	-0.081
Relative and % changes with and without pom and bc in no ship with Dalsoren and Dentener emission									
-0.010	16%	0.00001	50%	0.06	33%	0.0039E(+6)	15%	0.007	18%
-0.01	8%	0.00001	50%	0.06	19%	0.0039E(+6)	9%	0.008	11%

Table (7) gives the detailed brief explanation on the influence of some of the constituents shipping emissions including POM and BC on the radiative and microphysical properties of cloud, where their net effect was to increase the ship induced SWCF by -0.01 Wm^{-2} equivalent to 8% and 16% depending upon the inventory. This value of model calculated global mean ship induced SWCF due to POM and BC is ten times lower than the contribution of only total anthropogenic BC on SWCF (of -0.1 Wm^{-2}) calculated by Kristjansson et al., 2002.

In the perspective of the difference in geographical distribution of the ship induced SWCF with and without POM and BC, figure 13(c)) show the highest difference ranging from -0.1 to -0.3Wm^{-2} is observed over Northern Atlantic Ocean, Mediterranean Sea and South Eastern Asia. Most of the traffic areas are mapped up with the difference of -0.05 Wm^{-2}, these areas includes Northern Atlantic and Pacific ship, Mediterranean Sea as well as Indian Ocean. Whereas SH is characterized by the mapping of less than -0.05Wm^{-2}, again indicating that not only for sulphate particles, but the ship induced effects on clouds and climate for POM and BC is also highly concentrated in NH mid to high latitudes .

4.10 Discussion

From previous sections we have seen that CAM3.0 simulation results for various microphysical and radiative parameters (including SWCF) differs with that of other recent studies including Lauer et al., 2007, whom used the E5/M1-MADE climate model to investigate the impact of ocean - going ships emitted (sulphate) aerosols, on clouds and the earth's radiation budget. Our concern in this section is to suggest or hypothesize and providing proved reasons which lead to these intra model differences in estimating the SWCF using the same emission inventory.

The model simulation results on global mean SWCF are -0.063 Wm^{-2} for CAM3.0 and -0.19 Wm^{-2} for E5/M1-MADE, indicating that the former is about three times lower than the letter. This factor of difference is not only for the global mean SWCF, but also for the SWCF over specified regions including Pacific and Atlantic Oceans.

Also the total indirect effect for all anthropogenic aerosols is -1.9Wm^{-2} for CAM3.0 (Hoose et al., 2009), and -1.1 Wm^{-2} to -1.5 Wm^{-2} for E5/M1-MADE (Lauer et al., 2007), indicating that CAM3.0 has higher total anthropogenic indirect effect than E5/M1-MADE. But using Dentener emission the % contribution of ship induced AIE to the total indirect effect of anthropogenic aerosols for CAM3.0 (3.3% to 6.4%) is lower by a factor of 5 than that of E5/M1-MADE (17%). This also supports our argument that E5/M1-MADE is more sensitive over Ocean than CAM3.0.

Among the suggested reasons that cause the high sensitivity of E5/M1-MADE over Ocean than CAM3.0 is based on aerosols scheme, that E5/M1-MADE has got higher percentage increase of accumulation mode size particle number concentration, which act as efficient condensation nuclei for cloud droplet formation (Eyring et al., 2009) than CAM3.0. Whereas in CAM3.0 aerosol number concentration and size distributions of sulphate (aerosol scheme) particles mainly condenses on pre-existing sea salt particles and create relatively few new accumulation mode particles which are in suitable size for activation.

In quantifying this (first reason) argument the model (CAM3.0) calculated the percentage contribution of accumulation size mode number concentration for the lowest boundary model layer over the land masked Atlantic Ocean. The model results show an increase of only 3%, where as E5/M1-MADE have the result of 15% (Lauer et al., 2007) increase in this size mode, indicating that CAM3.0 result is five times lower.

For the Aitken mode number concentration of exactly less than 0.1 μm, we used the nucleation mode size number concentrations which are very important for the model (CAM3.0) Storelvmo et al., 2007, and calculate the percentage contribution of these particles. The results give an increase of only 9% for CAM3.0, where as E5/M1-MADE have an increase of 40% (in approximate ratio of 1:4) for the same area and inventory. For the mean geometric diameter of these particles (Aitken less than 0.1μm) over the Atlantic Ocean at lower latitude (model levels 23, 24, 25), we used the same particles and the results were the decrease from 0.050 μm to 0.055 μm for CAM3.0, where as that of E5/M1-MADE are the decrease from 0.05 μm to 0.04 μm depending upon the inventory**.**

Due to the fact that CDNC depends more on the size of CCN and LWC (supper saturation level), the above lower boundary microphysical and radiative results play as the main reason for the E5/M1-MADE to higher relative and percentage changes in CDNC as well as LWP.

In view of this argument (as the second reason) we have compared the two model results for the relative and percentage changes of both microphysical and radiative parameters including ΔN and $\%\Delta N$, ΔLWP and $\%\Delta LWP$ and ΔR_e and $\%\Delta R_e$. Using these two models results at localized oceanic areas including the Pacific and Atlantic Oceans, as presented in tables (3(b) and 3(c)). These tables show that the % changes of CDNC for E5/M1-MADE are (5-10%) over Pacific Ocean and (20-30%) over the Atlantic Ocean but for the same areas and levels CAM3.0 have lower % changes of (2.92-2.51%) over Pacific Ocean and (3.69-3.19%) over Atlantic Ocean.

In case of % changes of cloud LWP for the selected areas E5/M1-MADE has a general change of (1-2%) but CAM3.0 has smaller changes of (0.34-0.41%) which are less than 1% the lower limit of E5/M1-MADE. For the % changes ΔR_e over the selected areas CAM3.0 have slight higher values than that of E5/M1-MADE. Also tables (2(a), 2(b) and 3(a)) provide the same comparison that E5/M1- MADE have higher relative and percentage changes in CDNC than CAM3.0, but CAM3.0 have relatively higher changes in R_e.

Since it is well agreed that SWCF or (AIE) largely depends on the relative and percentage ΔR_e and $\%\Delta R_e$ and ΔLWP and $\%\Delta LWP$ which depends on the change of ΔN and $\%\Delta N$. These listed parameters are well related by equations (2, 3, 4, 5 and 6), that for a fixed value of LWC the increase in CDNC should be associated with the increase in column LWP followed by the decrease in R_e (due to competition effect for the existing LWC) which enhances the increase in CA (i.e. due to increase in cloud droplet surface area Kristjansson et al., 2002) and hence the cloud shortwave response.

In connection with the conclusions made from sections (4.6.1, 4.5.1 and 4.4.1 and the used examples which are supported by the above mentioned equations we can generally conclude that **"**since E5/M1-MADE has higher relative and percentage changes in ΔN and $\%\Delta N$ which increases oceanward and higher percentage changes $\%\Delta LWP$ associated with approximately equivalent relative and percentage changes in ΔR_e and $\%\Delta R_e$ as CAM3.0, but in contrary CAM3.0 has lower changes in ΔN and $\%\Delta N$ which decreases Oceanward and lower percentage changes in $\%\Delta LWP$ associated with slightly higher changes in ΔR_e and $\%\Delta R_e$ which increases Oceanward, it is logically acceptable for CAM3.0 results of SWCF to be 3 times lower than that of E5/M1-MADE."

The influence of POM and BC (as the third reason) we have seen from section 4.9 that these organics has raised the AIE results from 0.063 Wm^{-2} to **-0.**073 Wm^{-2} indicating that they have the contribution of about 0.01Wm^{-2}. On comparing this CAM3.0 result of -0.073 Wm^{-2} and that of E5/M1-MADE(-0.19 W/m^2) you will notice that still E5/M1-MADE result of using Dentener shipping inventory is large than for CAM3.0, but the multiple factor has been reduced from 3 times lower to 2.6 times lower.

Hence from these results we conclude that, running the model with POM and BC in the no ship emission(i.e. the back ground or pre- industrial emisssions) is another factor or reason which contributed the CAM3.0 results to be 3 times lower than that of E5/M1-MADE.

CHAPTER FIVE

PERTURBATION RESULTS

5.0 Perturbation of cloud parameters with sulphur emission

In this chapter we have presented the results of experiment dealt on perturbing the change in cloud parameters with the change in sulphur emission. The results of this experiment reflects the findings by Taylor et al., 1997 that the impact of the aerosol emitted from ships is very dependent on the background cloud microphysical conditions.

In view of this we have perturbed the changes in cloud droplet effective radius (ΔR_e), cloud droplet concentration number Δ(CDNC) or ΔN, the cloud integrated liquid water path ΔLWP and the combined net effect of the changes in their parameters i.e. the short wave cloud forcing Δ(SWCF) with the changes in the back ground sulphur emission $\Delta(SO_2)$ i.e. ship induced sulphur emission.

The results reflects great respond of both cloud properties over areas which are clean followed by areas with low emission levels and common ship route areas have shown less response

5.1 Perturbation of cloud droplet number concentration with sulphur emission

Figure 15(a)

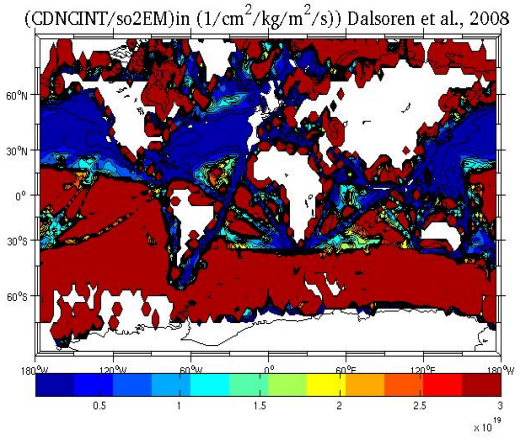

Figure 15(b)

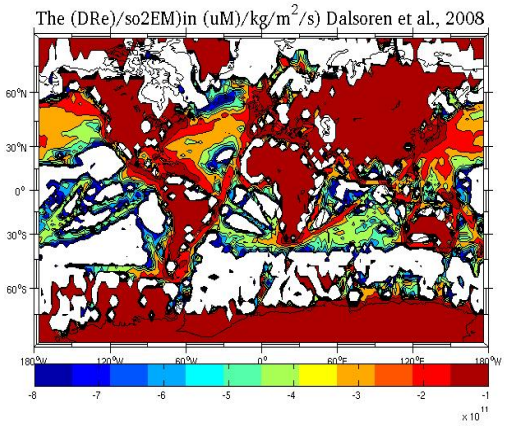

Figures 15(a-b) the annual geographical distribution of the perturbation of column ($\Delta N/\Delta So_2$) and ($\Delta R_e/\Delta SO_2$) changes due to Dalsoren et al., 2008 .Note in both figure areas white have either zeros or infinitely large values (which have been set to be zeros)

The perturbation of sulphur emission with integrated cloud droplet number concentration ($\Delta N/\Delta SO_2$) shows the highest effects over the areas away from shipping routes i.e. areas which has little extent of pollution. This is shown figure 15(a) that its highest effects (large values) is mapped over the regions which are out of the shipping routes and remote Oceans,

and less effects over the main shipping routes. On this sensitivity experiment the Southern Oceans are seen to be more affected as compared to northern Oceans, which in turn (the opposite is true) support our argument of having more microphysical and radiative effects due to shipping emission on the NH than SH.

5.2 Perturbation with cloud droplet effective radius

The results of perturbation of ($\Delta R_e/\Delta SO_2$) sensitivity show similar but opposite effect as the CDNC, figure 7(b) apart from showing the less effect (reduction in R_e) on the remote oceans and less frequent shipping areas but also it shows clearly the shipping routes and the intensity of their effect at every point especially over the SH. In this figure SH seems to be less sensitive to changes in effective radius than NH, this is because emission level and the changes in radius due to shipping is very small over most remote Oceanic areas including that of SH. The highly polluted areas have been more sensitive because the decrease in cloud sizes is higher in these areas than in remote and less polluted areas. Otherwise we can conclude that the perturbation of changes in cloud droplet effective radius with changes in emission is not a good indicator for sensitivity.

5.3 Perturbation with cloud integrated liquid water path. ($\Delta LWP/\Delta SO_2$)

The cloud liquid water path is very dependent on the activated CDNC (equation 2 and 4), therefore its perturbation changes in sulphur emission is expected to show similar results (pattern) to that of CDNC. Figure 16(a) reflects the Taylor's findings by mapping highly polluted areas with low values indicating that they are less sensitive due to their high back ground level of CDNC and LWP, where as the remote and less polluted have been mapped with high values indicating that they are sensitive to changes in cloud back ground caused by injected pollutants from shipping. This means that the increased response to the increase in LWP (due to emission change) over the polluted areas is lower than over the less polluted remote Oceanic areas.

Figure 16(a)

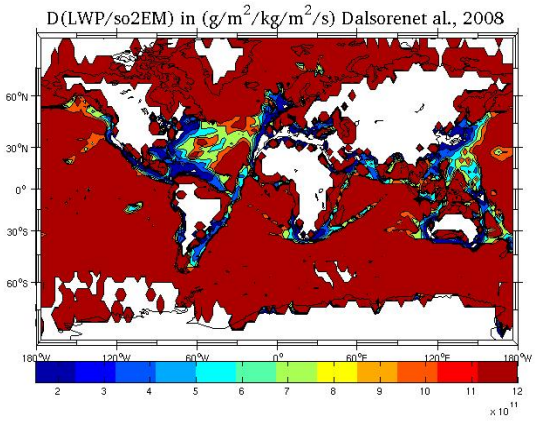

Figure 16 (b)

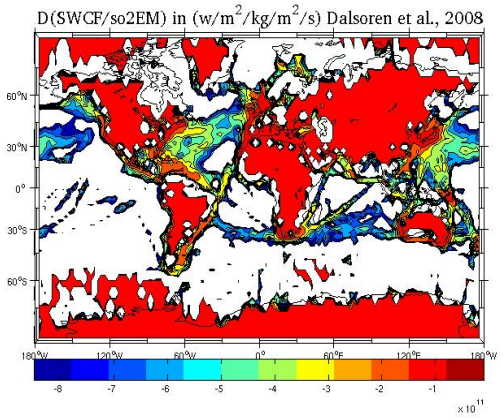

Figure 16 (a-b); perturbation result in Δ(LPW) by Δ(so_2). Note in both figures white are either zeros or infinitely large numbers (which has been set to be zeros)

5.4 Perturbation with short wave cloud forcing ($\Delta SWCF/\Delta SO_2$)

The results of this sensitivity might have been influenced by the sensitivities of both the effective radius and the liquid water path to the sulphur emission i.e. ($\Delta R_e/\Delta so_2$) and ($\Delta LWP/\Delta So_2$), and will follow the combined pattern of the two parameters.

The interpretation to the figure 16(b) is that areas with low values are the sensitive ones because their value for ($\Delta SWCF$) are low and that of (ΔSO_2) are also low causing the lower changes but areas which have mapped with high values or less sensitive because the areas have got high changes in shortwave cloud forcing induced by high changes in emission causing high values to be mapped indicating high back ground emission areas hence the less sensitive. Here we also conclude that the perturbation of the changes in SWCF, with the changes in emission is not a straight forward indicator for the sensitivity.

5.5 Brief summary for this chapter

In this chapter we have looked on the respond on the emission change for the areas with low back ground cloud properties including the CDNC and LWP, but are associated with high values for cloud droplet effective radius.

We have perturbed the ship induced changes in LWP, CDNC, R_e and SWCF ($\Delta CDNC$, ΔLWP, ΔRe and $\Delta SWCF$) with only sulphur emission from shipping (ΔSO_2). The results for this perturbation have shown that for $\Delta CDNC$ and ΔLWP are in agreement with Taylor's finding that remote areas are more sensitive than common ship traffic areas (in these areas the response decreases with the increasing CDNC and LWP). Because these areas have very low ship induced changes in LWP and CDNC (refer figure 7(a) and 12(a)) and they are

climatologically with less CDNC and LWP due anthropogenic sulphate aerosols, as agreed by Kristjansson et al., 2002 that these areas have the integrated LWP due to anthropogenic sulphate aerosols of less than 0.5 gm^{-2}

For the perturbation of ship induced effective radius and SWCF over these areas the results are either opposite to that of CDNC and LWP because ΔR_e, ΔSWCF and ΔSO_2 are small (refer figure 1(a), figure 9(a) and figure13 (a) as in agreement with Kristjansson et al., 20002, or the perturbation of changes of these two parameters with changes in emission is not a suitable or direct indicator for the susceptibility experiments.

CHAPTER SIX

SUMMARY OF FINDINGS AND FINAL COMMENTS

6.1 Summary of the findings

In this study we have used the Community Atmosphere Model version three (CAM3.0) to investigate the impact of sulphate (emitted from the ocean - going ships) to clouds and climate. Global climate models with double-moment aerosol and detailed cloud microphysics schemes CAM3.0 which is particularly well suited for the calculation of aerosol indirect effects have allowed the assessment of the aerosol indirect effect due to sulphate particle and organics (POM and BC) from the shipping emission to be performed. The model out puts has been detailed analyzed on contexts of annual, seasonal, zonal variations and hemispherical fluctuations, where as the geographical distribution of the shipping effects on microphysical and radiative properties of clouds has been mapped.

To avoid the cloud microphysical and radiative effects to feed back into the model meteorology the offline simulations for the 2001 (present-day conditions) has been conducted. In assessing the data (emissions) uncertainty which influence the uncertainty of the results (AIE), two shipping emission inventories Dentener et al., 2006 and Dalsoren et al., 2008 have been used. The ship induced microphysical and radiative impacts including the particle number concentration, size distribution aerosols optical thickness est. has been calculated by taking the differences from the runs i.e. the difference between model runs without ship and those with ship emissions.

The study have only looked the indirect effect (first kind and second kind but not separately) of sulphate emissions from ships. Further more for checking the performance of the model we compared the results with that obtained by E5/M1-MADE (Lauer et al., 2007), and suggest possible reasons for the difference in the two models results.

The model calculated percentage ship induced sulphate burden is 3.0% to 3.8% of the total atmospheric sulphate burden in the simulations with Dentener and Dalsoren emissions. In case of BC and POM the ship induced percentage burden are 2.0% and 0.5% of the total BC and POM in the atmosphere. On the aspect of number concentration and particle size distribution, the study was more interested over the Atlantic Ocean where the results of the percentage ship induced accumulation mode particle number concentration near the surface is only 3% to 6%, where as for the Aitken mode particle number concentration on the same area and level the model results are 9% to 10% indicating small percentage of the ship induced particle number concentration suitable for CCN

The model result of the relative and percentage decrease of the geometrical mean diameter of the Aitken particle (typically less than 0.1μm) over this area is 0.050 μm and 0.055 μm equivalent to 3.9% and 4% based on the inventory.

The global mean impact of the emissions from international shipping traffic on the Earth's radiation budget caused by ship induced cloud microphysical properties are -0.063 Wm^{-2} to -0.121 Wm^{-2} for simulations with POM and BC on the model back ground or (pre–industrial emission), when removing these particles the impact has risen up to -0.073 Wm^{-2} and -0.131 Wm^{-2} indicating that POM and BC has increased the impacts by -0.01 Wm^{-2} equivalent to 16% and 8%. For the frequent shipping traffic areas including the Atlantic and Pacific Oceans the ship induced impact on the Earth's radiation budget is -0.188 Wm^{-2} to -0.242 Wm^{-2} for Atlantic Ocean and -0.143 Wm^{-2} to -0.185 Wm^{-2} for Pacific Ocean. These higher values of the AIE show the extent to which these areas are susceptible to increase aerosol number concentration or burden.

For seasonal variation the highest ship induced impact on the Earth's radiation budget was found on JJA seasonal period with model results of -0.102 Wm^{-2} to -0.187 Wm^{-2} for simulations with POM and BC and -0.112 Wm^{-2} to -0.197 Wm^{-2} for simulations without POM and BC. This can not only be explained by the slightly observed northward shift of the shipping traffic during this period of the year, but also the increase in CA, amount of radiation and insolation time which largely depends on the solar zenith angle.

On the Hemispherical basis the NH have high ship induced influence on the earth's radiation budget, but increased ship traffic to the SH has induced the increase of the impact from -0.021 Wm^{-2} to -0.065 Wm^{-2} for the simulations with POM and BC, and -0.024 Wm^{-2} to -0.068 Wm^{-2} for the simulation without POM and BC, indicating that the increase by a factor of 2.8 to 3.1 times the impact caused by Dentener shipping emissions. The study has found the global mean ship-induced decrease in R_e by about 0.0395 μm to 0.0738 μm causing an increase in COD by (0.0583 to 0.098) and hence enhance the change in CA by (0.0008 to 0.0016).

Through different sensitivity experiments, the study has found that areas characterized by low level liquid water clouds are more affected by shipping traffic (due to their sensitivity to increased aerosols number concentration), these areas include North western Pacific Ocean (areas of Tehuantepec Bay and Californian Gulf), North western Atlantic Ocean (areas of Gulf of Mexico), and all most the entire north eastern Atlantic Ocean including areas of Baltic and North Sea, English Channel and the coast of Portugal, Spain and the Northwestern Africa at the western boarder of Morocco and Spain where the Mediterranean Sea channels in land . For the southern Atlantic, areas of west coast of southern Africa has shown significant impact, where as for the Indian Ocean areas of Gulf of Aden est. have been among the impacted ones.

Apart from the global and season effects also the study investigate the latitudinal impact of the shipping emissions, where the results reflects the findings by previous studies including Eyring et al., 2009; Wang et al., 2007 and Endresen et al., 2003 that the NH especially at mid to high latitude zones has been more affected compared to SH. But the results from Dalsoren emission inventory has shown an increase of short wave radiative effect to about 3.1 times that of Dentener emission inventory, indicating the increase of the ship induced pollutants, and hence reducing the confidence of the idea that the SH is still among pristine areas.

Furthermore the southern high latitudes including the Antarctica which was believed to be most pristine has shown a radiative impact of about -0.05 Wm^{-2} to the Earth's radiative budget over DJF seasonal period, but still it is less affected than the NH Arctic. Over the tropical Oceans the study has also found a significant shipping impact with Northern Tropical Oceans being more affected than the southern. On the aspect susceptibility due to emission change the simulation results reflects the dependency on the back ground emission, where infrequent ship traffic areas including the remote Ocean have shown to be more susceptible than the frequent ship traffic area.

On comparing the results from other studies dealing with the impact of ship traffic on microphysical and radiative properties of cloud and climate (Lauer et al., 2007), the intra model results i.e. CAM3.0 and E5/M1-MADE on the ship induced aerosol indirect effect was in the ratio of 1:3 **(**the CAM3.0 results was three times lower than the E5/M1-MADE). Among other reasons this has been contributed by CAM3.0 results of low percentage increase in accumulation mode number concentration at the Atlantic Ocean (i.e. 3% as to 15% the ratio of 1:5), and an increase of only 9% of Aitken size mode (of exactly less than 1μm) than 40% of E5/M1-MADE, at the lowest boundary layer above shipping routes.

The study investigated both relative and percentage changes in CDNC and R_e and found that, for the same area, level and emission inventory, the E5/M1-MADE have higher oceanward increase in relative and percentage changes in CDNC than CAM3.0, which has shown to have slightly higher oceanward increase in relative and percentage changes in R_e. Based on these results the study has found that, the uncertainty on the overall AIE is mainly determined by two major factors i.e. emissions inventories and models (model differences in chemistry and aerosols activation schemes)

6.2 Final comments

Based on different results from the two used emission inventories and the model comparisons, the study comments that the uncertainty on the ship induced AIE is not only brought by the uncertainty in shipping emissions inventories, but also the model differences i.e. estimates of indirect aerosol forcing are mainly model-based and highly uncertain.

Without doubt this study and the earlier ones including Lauer et al., 2007; Collins et al., 2008 and Eyring et al., 2009, has come to a common point that emission totals due to shipping traffic are increasing causing the increase in AIE which have a great influence to the redistribution of the balanced earths radiation budget and hence affect the climate system, so there is a need to reduce ship induced emission levels.

Though there is an increasing concern in the study of ship induced influence on clouds and climate, there are more challenges including standard and common guidelines for modeling of ship emission inventory, detailed modeled aerosols schemes with in significant intra model variability and extensive knowledge of aerosols behavior in different atmospheric conditions (aerosols show a large variability in their physical, chemical and optical properties). The solution to these challenges can reduce the existing uncertainties due to present modeled inventories, and modeled aerosols schemes.

For further study on the influence of ship emissions to clouds and climate the study proposes the following to be done;

(i) The study has only quantified the influence of ship induced sulphate, BC and POM to microphysical and radiative properties of cloud (only indirect effect), since other ship emitted particles also have the influence to clouds and climate, there is a need for more research work to investigate the total atmosphere (direct and indirect) impact of ship emission using the CAM3.0

(ii) SH has shown to be sensitive to emission changes, which are enhanced by annually increasing emission rates due to growth of ship traffic (Eyeing et al., 2009) caused by increasing world sea trade. Since the atmosphere has no boundaries, more research work is required to investigate the influence ship emitted pollutants on clouds and climate over SH. But regional climate models (RCM) which can simulate exact SH atmospheric conditions should be used instead of global climate models (GCM).

REFERENCES

Abdul-Razzak, H., and S. J. Ghan (2000), A parameterization of aerosol activation: 2. Multiple aerosol types, J. Geophys. Res., 105, 6837–6844.

Abdul-Razzak, H., and S. J. Ghan (2002), A parameterization of aerosol activation: 3. Sectional representation, J. Geophys. Res., 107(D3), 4026, doi: 10.1029/2001JD000483.

Abdul-Razzak, H., S. Ghan, and C. Rivera-Carpio (1998), A parameterization of aerosol activation: 1. Single aerosol type, J. Geophys. Res., 103, 6123–6131.

Anttila, T and Kerminen, V. M : The influence of organic compounds on the cloud droplet activation, A model investigation considering the volatility, water solubility and surface activity of organic matter. J. Geophys, Res.-Atmos., 107,4662.doi:10.1029/2001JD00148, 2002.

Albrecht, B.: Aerosols, Cloud Microphysics, and Fractional Cloudiness, Science, 245, 1227-1230, 1989.

Barkstrom, B. R.: The Earth Radiation Budget Experiment (ERBE), Bull. Amer. Meteor. Soc., 65, 1170–1185, 1984.

Beheng, K. D. (1994), A parameterization of warm cloud microphysical Conversion processes, Atmos. Res., 33, 193–206.

Bennartz, R., Global assessment of marine boundary layer cloud droplet number concentration from satellite, J. Geophys. Res. 112, D02201, doi: 10.1029/2006JD007547, 2007.

Bilde, M. and Svenningson, B.: CCN activation of slightly soluble organics: the importance of small amount of ignoring salt and particle phase, Tellus B, 56,128-134, 2004.

Boucher, O., and Lohman, U. The sulphate –CCN cloud albedo effect: A sensitivity study with two general ciculation models , Tellus, 47B, 281-300, 1995.

Capaldo, Kevin., James , J. Corbett., Prasad Kasibatia., Paul, Fiscbeck and Spyros N. Pandis., 1999, effects of ship emission on sulphur cycling and radiative climate forcing over the Ocean; Nature vol 400 19Aug 2009.

Coakley and Walsh 2002, Limits to the Aerosol Indirect Radiative Effect Derived from Observations of Ship Tracks, Journal of the atmospheric sciences volume 59.

Collins, W.J., Sanderson, M.G., Johnson, C.E., 2009. Impact of increasing ship emissions on air quality and deposition over Europe by 2030, Meteorologische Zeitschrift, Meteorologische Zeitschrift 18 (1), pp. 25–39(15) Conover, J. H., 1966, Journal of Atmospheric Science 23, 778–785.

Clollins, W. D., Rasch P. J., Bovvile, B. A., Jamea J. H, James R. M., David L. W. and Bruce P. B. 2006, The Formulation and Atmospheric Simulation of the Community Atmosphere Model **Version 3 (CAM3),** JOURNAL OF CLIMATE VOLUME 19

Dalsoren1 S. B., M. S. Eide, Ø. Endresen, A. Mjelde, G. Gravir, and I. S. A. Isaksen1, Update on emissions and environmental impacts from the international fleet of ships the contribution from major ship types and ports; Atmos. Chem. Phys. Discuss., 8, 18323–18384, 2008

Dentener, F., S. Kinne, T. Bond, O. Boucher, J. Cofala, S. Generoso, P. Ginoux, S. Gong, J. J. Hoelzemann ,A. Ito, L. Marelli, J. E. Penner, J.-P. Putaud, C. Textor, M. Schulz, G. R. van der Werf, and J.Wilson, Emissions of primary aerosol and precursor gases in the years 2000 and 1750 prescribed data-sets for AeroCom; Atmos. Chem. Phys., 6, 4321–4344, 2006.

Dick, W. D, Estimation of water up takes by organic compounds in submicron aerosols measured during the Southern Aerosol and Visibility study, J. Geophys. Res., 105, 1471-1479, 2000.

Durkee, P. A., Chartier, R. E., Brown, A., Trehubenko, E. J., Rogerson, S. D., Skupniewicz, C., Nielsen, K. E., Platnick, S., and King, M. D.: Composite Ship-Track Characteristics, J. Atmos. Sci., 57, 2542–2553, 2000.

EPA (Environmental Protection Agency, U.S.A.), 2006: SPECIAL 3.2, Profiles of Total Organic Compounds and Particulate Matter. http://www.epa.gov/ttn/chief/ software/speciate/index.html.

Endresen, Ø., Bakke, J., Sørgård, E., Berglen, T.F., Holmvang, P., 2005, Improved modeling of ship SO2 emissions – a fuel based approach. Atmospheric Environment 39, 3621–3628

Erickson, D.J., Oglesby, R. J., and Susan Marshall, S., : Climate response to indirect anthropogenic sulfate forcing Geophysical research letters, vol. 22, NO. 15, PP. 2017-2020, 1995 doi: 10.1029/95GL01660

Eyring, Veronica., Ivan S.A. Isaksen , Terje Berntsen , William J. Collins , James J. Corbett, Øyvind Endresen , Roy G. Grainger , Jana Moldanova , Hans Schlager , David S. Stevenson, Transport impacts on atmosphere and climate: Shipping, Atmospheric Environment xxx (2009) 1–37.

Eyring, V., Ko¨ hler, H.W., Lauer, A., Lemper, B., 2005b. Emissions from international shipping: 2. Impact of future technologies on scenarios until 2050. Journal of Geophysical Research 110, D17306. doi:10.1029/2004JD005620.

Eyring, V., Ko¨ hler, H.W., van Aardenne, J., Lauer, A., 2005a. Emissions from international shipping: 1. The last 50 years. J. Geophys. Res.110, D17305. doi:10.1029/ 2004JD005619

Facchini , M. C., Fazzi, S., ZAppoli, S., Andracchio, A., Gelencser, A., Kiss, G., Krivacsy, Z,. Meszaros, E,. Hansoon , H. C., Alsber , T.. and Zebuhr , Y., Partitioning of the organic aerosol component between dog droplrt abd interstitial air , J. Geophys. Res-Atmos, 104, 261821–26332, 1999.

Fearnleys, 2007. (Fearnleys Review 2007), the Tankerand Bulk Marketsand Fleets, Oslo

Feichter, J., Roeckner, E., Lohmann, U. and Liepert, B. 2004. Nonlinear aspects of the climate response to greenhouse gas and aerosol forcing. *J. Climate* **17**, 2384–2398.

Hasselmann, K., 1993; Optimal fingerprints for the detection of time dependent climate change. *J. Climate*, **6,** 1957–1971 , and Coauthors, 1995: Detection of anthropogenic climate change using a fingerprint method. MPI Rep. No. 168, 24 pp.

Han. Q., Rossow, W. B., Chou, J., Welch, R. M. J. Global variations of column droplet concentrationin low level cloud Geophys Res lett., 27,3221-3224.

Haywood, J.M., V. Ramaswamy, and L.J. Donner, 1997b: A limited-area-model case study

of the effects of sub-grid scale variations in relative humidity and cloud upon the direct radiative forcing of sulfate aerosol. Geophys. Res. Lett., **24**, 143-146.

Holben, B., Eck, T., Slutsker, I., Tanre, D., Buis, J., Vermote, E., Reagan, J., Kaufman, Y., Nakajima, T., Lavevau, F., Jankowiak, I., and Smirnov, A.: AERONET – A federated instrument network and data archive for aerosol characterization, Rem. Sens. Environ., 66, 1–16, 1998.

Hobbs, P. V., Garrett, T. J., Ferek, R. J., Strader, S. R., Hegg, D. A., Frick, G. M., Hoppel, W. A., Gasparovic, R. F., Russel, L. M., Johnson, D. W., O'Dowd, C., Durkee, P. A., Nielsen, K. E., and Innis, G., Emissions from ships with their respect to clouds, J. Atmos. Sci., 57, 2570–2590, 2000.

Hoose, C., J. E. Kristjansson, T. Iversen, A. Kirkevaag, Ø. Seland, and A Gettelman , constraining cloud droplet concentration geophysical research letters, vol. 36, l12807, doi:10.1029/2009gl038568, 2009.

Jones, A., and A. Slingo, 1996: Predicting cloud droplet effective radius and indirect sulphate aerosol forcing using a general circulation model. *Quart. J. Roy. Meteor. Soc.,* **122,** 1573–1595.

Johns, T. C., R. E. Carnell, J. F. Crossley, J. M. Gregory, J. F. B.Mitchell, C. A. Senior, S. F. B. Tett, and R. A. Wood, 1997: The second Hadley Centre coupled model ocean–atmosphere GCM: Model description, spinup, and validation. *Climate Dyn.,* in press.

Kazuaki Kawamotoa, Tadahiro Hayasakaa, Teruyuki Nakajimab David Streetsc, Jung-Hun Wood , Examining the aerosol indirect effect over China using an SO2 emission inventory Atmospheric Research 72 (2004) 353–363.

Khairoutdinov, M. and Kogan, Y.: A new cloud physics parameterization in a large eddy simulation model of marine stratocumulus, Mon. Weather Rev., 128, 229–243, 2000.

Kirkevaag, A., T. Iversen, Ø. Seland, J. B. Debernard, T. Storelvmo, and J. E. Kristjansson (2008), Aerosol-cloud-climate interactions in the climate model CAM-Oslo, Tellus Ser. A, 60, 492– 512.

Kinne, S., Schulz, M., Textor, C., Guibert, S., Balkanski, Y. and coauthors. 2006. An AeroCom initial assessment – optical properties in aerosol component modules of global models. *Atm. Chem. Phys.* **6**, 1815–1834

Kristjansson, J. E., (2002), Studies of aerosol indirect effect from sulphate and black carbon aerosols, J, Geophysics. Res., 107(D15), 4246, doi: 10.1029/2001JD000887.

Kristjansson, J. E., Iversen, T., Kirkevag, A., Selad , O. and Debernard, J. 2005. Response of climate system to aerosol direct and indirect forcing , Role of cloud feed backs. J. Geophysics. Res. 110D24206, doi: 10.1029/2005JD006299.

K. Krishna Moorthy and S. Suresh Babu, Aerosol Characteristics and Radiative Impacts over the Arabian Sea during the Intermonsoon Season: Results from ARMEX Field Campaign Journal of the Atmospheric Sciences, 2005; 62: 192-206

Lacis A.A. and Hansen, J. E. Parameterization for the absorption of solar radiation in the Earth's Atmosphere. J. Atmos. Sci. 31,118 -133.

Lauer, A., V. Eyring1, J. Hendricks, P. J¨ockel, and U. Lohmann, Global model simulations

of the impact of ocean-going ships on aerosols, clouds, and the radiation budget; Atmos. Chem. Phys., 7, 5061–5079, 2007.

Lohmann and J. Fleichter 2005; Global indirect aerosol effects (a review) Atmos. Chem. Phys., 5, 715–737, 2005

Lohmann, U., Fleichter, J., Chuang, C. C., and Penner, J. E.: Prediction of the number of cloud droplets in the ECHAM GCM, J. Geophys. Res., 104, 9169–9198, 1999.

Lohmann, U., P. Stier, C. Hoose, S. Ferrachat, S. Kloster, E. Roeckner, and J. Zhang (2007), Cloud microphysics and aerosol indirect effects in the global climate model ECHAM5-HAM, Atmos. Chem. Phys., 7, 3425–3446.

Lohmann .U Broekhuizen, K., Leaitch, R., Shantz, N.,and Abbat,J., How efficient is cloud droplet formation of organic aerosols, Geophy, Res. Lett., 31, L05108, doi:10.1029/2003GL018999,2004.

Lubin, Dan., & Andrew M. Vogelmann A climatologically significant aerosol long wave indirect effect in the Arctic, letters nature/Vol 439|26 January 2006|doi:10.1038/nature 04449

Mitchell R. A. Davis, W. J. Ingram, and C. A. Senior, 1995a: On surface temperature, greenhouse gases, and aerosols, Models and observations. *J. Climate,* 8**,** 2364–2386.

Mittchell, T. C. Johns, J. M. Gregory, and S. F. B. Tett, 1995b: Climate response to increasing levels of greenhouse gases and sulphate aerosols. *Nature,* 376**,** 501–504

Morrison, H and Gettelman, A. 2008 : A New Two-Moment Bulk Stratiform Cloud Microphysics Scheme in the CommunityAtmosphere Model, Version 3 (CAM3). Part I: Description and Numerical Tests JOURNAL OF CLIMATE VOLUME 21

Olivier, J. G. J., van Aardenne, J. A., Dentener, F., Ganzeveld, L., and Peters, J. A. H. W.: Recent trends in global greenhouse gas emissions: regional trends and spatial distribution of key sources, in: Non-CO2 Greenhouse Gases (NCGG-4), van Amstel, A. (coord.), 325–330, Millpress, Rotterdam, ISBN 90 5966 043 9, 2005.

Penner, J. E., Quaas, J., Storelvmo, T., Takemura, T., Boucher, O. and co-authors, 2006: Model intercomparison of indirect aerosol effects, *Atm. Chem. Phys.* **6**, 3391–340.

Rasch, P. J. and Kristjansson, J. E., A comparison of the CCM3 model climate using diagnosed and predicted condensate parameterizations, J. Climate, 11, 1587–1614, 1998.

Roeckner, E., Bengtsson, L., Feichter, J., Lelieveld, J., and Rodhe, H., Transient Climate Change Simulations with a Coupled Atmosphere-Ocean GCM Including the Tropospheric Sulfur Cycle, J. Climate, 12, 3004–3032, 1999.

Rotstayn, L. D. and Liu, Y., Sensitivity of the first indirect aerosol effect to an increase of cloud droplet spectral dispersion with droplet number concentration, J. Climate, 16, 3476–3481, 2003.

Seland, Ø., Iversen, T., Kirkervag, A., Storelvmo, T., 2007; Aerosol-climate interactions in the CAM-Oslo atmospheric GCM and investigation of associated basic shortcomings; Tellus (2008) 60A, 459-49I.

Sekiguchi, M., Nakijima, T., Kawamoto, K., Higurashi, A., Rosenfeld, D., Sno, I., Mukai, S. 2003, A study of the direct and indirect effects of aerosols using global satellite data sets of aerosols and cloud parameters; J. Geophy, vol No. D22, 4699, doi: 1029/2002JD003359,

2003.
Shantz, N. C., Leiatch, W. R., Mozurkewich, M., Toom-Santry, D. 2008; The effect of organic compounds on the growth rate of cloud droplets in marine and forest settings; Atmos. Chem. Phys., 8, 5869-5887
Shulman, M., Jacobson, M. C., Calson,R. J., Synoes, R. E., and Young ,T. E., Dissolution behavior and surface tension of organic compounds in nucleating the cloud droplets, Geophys, Ress. Lett. 23, 277-280, 1996.
Shirsat and Graft 2009; Emission inventory of sulphur from anthropogenic sources in Antarctica; Atmos. Chem.,Phys., 9,3397-3408,2009.
Slingo, A., 1989, A GCM parameterization for the short wave radiative properties of water clouds. *J. Atmos. Sci.,* 46**,** 1419–1427.
Storelvmo, Trude Jon Egill Kristja´nsson, Steven J. Ghan, Alf Kirkevaag, Øyvind Seland, and Trond Iversen ; Predicting cloud droplet number concentration in Community Atmosphere Model (CAM)-Oslo; JOURNAL OF GEOPHYSICAL RESEARCH, VOL. 111, D24208, doi: 10.1029/2005JD006300, 2006
Taylor, Jonathan P., Martin D. Glew., James A., Coakley Jr., William R.. Tahnk Steven Platnick., Peter V. Hobbs., and Ronald J. Ferek., effects of aerosols on the radiative properties of clouds; journal of the atmospheric science s volume 57
Taylor, K. E. and Penner, J. E.: Response of the climate system to atmospheric aerosols and greenhouse gases *Nature* 369, 734 - 737 (30 June 1994); doi:10.1038/369734a0
Twomey, S. A., The influence of pollution on the shortwave albedo of clouds, J. Atmos. Sci., 34, 1149–1152, 1977.
Twomey S., Howell, H. E., Wajciechowski, T.A., Comments on anomoulous cloud lines, J, Atmos Sci., 25, 333-334, 1968.
Wang, M and Penner, J.E,. Aerosol indirect forcing in a global model with particle nucleation **Atmos**. Chem. Phys., 9, 239-260, 2009 www.atmos-chem phys.net/9/239/2009/ doi: 10.5194/acp-9-239-2009
Wang, J., Lee, Y.-N., Daum, P. H., Alexander, M. L., 2008; Effects of aerosols organics on cloud condensation nucleus concentrations and first indirect effect; Atmos. Chem., Phys. 8,6325-6339,2008

Appendix A

These map sections have names which have been used in this study at deferent sections of this study so we have presented them in for the reader to have a clear image of shipping traffics and their effects


RED SEA
©GraphicMaps.com
Lebanon
Syria
Damascus
Baghdad
Iran
Mediterranean Sea
Israel
Amman
Jerusalem
Port Said
Suez Canal
Suez
Cairo
Jordan River
Iraq
Jordan
Elat
SINAI
Gulf of Suez
Gulf of Aqaba
Kuwait
Jamsah
Al Ghardaqah
Sharm al-Sheikh
160 mi
160 km
Nile River
ASIA
Egypt
Medina
Riyadh
Aswan
AFRICA
Red Sea
Saudi Arabia
Sudan
Jedda
Mecca
Port Sudan
Nile River
Farasan Islands
Dahlak Archipelago
Asmara
Khartoum
Eritrea
Yemen
Sana
Bab el Mandeb
Aden
Blue Nile
White Nile
Hanish Islands
Djibouti
Gulf of Aden
Djibouti
Ethiopia
Somalia
©GraphicMaps.com


BAY OF BENGAL
©GraphicMaps.com
WorldAtlas.Com
Nepal
Bhutan
Bangladesh
Ganges
Dhaka
300 m
300 km
Kolkata (Calcutta)
Burma (Myanmar)
Mouths of the Ganges
Irrawaddy
India
Godavari
Visakhapatnam
Rangoon
Krishna
Bay of Bengal
Thailand
Mouths of the Irrawaddy
Chennai (Madras)
Andaman Islands (India)
Andaman Sea
Laccadive Sea
Cauvery
Malaysia
Arabian Sea
Sri Lanka
Nicobar Islands (India)
Gulf of Mannar
Indian Ocean
Indonesia (Sumatra)
Strait of Malacca


GULF OF ADEN
ASIA
WorldAtlas.Com
Saudi Arabia
Oman
125 mi
125 km
Al Ghaydah
Nishtun
Sana
Yemen
Sayhut
Al Hudaydah
Zabid
Al Mukalla
Arabian Sea
Red Sea
Eritrea
Aden
Gulf of Aden
(Sugutra)
Yemen
Bab el Mandeb
Djibouti
Djibouti
Boosaaso
Indian Ocean
Somalia
Hordio
Berbera
AFRICA
Ethiopia
©GraphicMaps.com